

## The Merging Galaxy Cluster Environment Affects the Morphology of Radio-AGN

MARY RICKEL <sup>1,2,3,\*</sup> EMILY MORAVEC <sup>1,†</sup> YJAN A. GORDON <sup>4</sup> MARTIN J. HARDCASTLE <sup>5</sup>  
JONATHON C. S. PIERCE <sup>5</sup> LAWRENCE E. BILTON <sup>6,7,8</sup> AND IAN D. ROBERTS <sup>9,10,11</sup>

<sup>1</sup>Green Bank Observatory, P.O. Box 2, Green Bank, WV 24944, USA

<sup>2</sup>Department of Astronomy, The Ohio State University, 140 West 18th Avenue, Columbus, OH 43210, USA

<sup>3</sup>Department of Physics, University of Notre Dame, Notre Dame, IN, USA

<sup>4</sup>Department of Physics, University of Wisconsin-Madison, 1150 University Ave., Madison, WI 53706, USA

<sup>5</sup>Department of Physics, Astronomy and Mathematics, University of Hertfordshire, College Lane, Hatfield, Hertfordshire AL10 9AB, UK

<sup>6</sup>Institute of Physics, Pontifical Catholic University of Valparaíso, Brasil 2950, Valparaíso, Chile

<sup>7</sup>Institute of Physics & Astronomy, University of Valparaíso, Blanco 951, Valparaíso, Chile

<sup>8</sup>Centre of Excellence for Data Science, Artificial Intelligence & Modelling, The University of Hull, Cottingham Road, Kingston-Upon-Hull, HU6 7RX, UK

<sup>9</sup>Department of Physics & Astronomy, University of Waterloo, Waterloo, ON N2L 3G1, Canada

<sup>10</sup>Waterloo Centre for Astrophysics, University of Waterloo, 200 University Ave W, Waterloo, ON N2L 3G1, Canada

<sup>11</sup>Leiden Observatory, Leiden University, P.O. Box 9513, 2300 RA Leiden, The Netherlands

(Received August 1st, 2024; Revised January 20th, 2025; Accepted February 4th, 2025)

### ABSTRACT

It has previously been found that the galaxy cluster environment can affect the fueling and evolution of Active Galactic Nuclei (AGN). This work examines the effect of the merging cluster environment on the properties of radio-AGN by comparing the radio morphology of cluster members in a sample of four merging and eight relaxed galaxy clusters at low redshift ( $z < 0.2$ ). Using 144-MHz data from the LOFAR Two-metre Sky Survey (LoTSS) and Zooniverse, we classify the radio morphology of the radio-detected cluster members using the following morphology classes: compact, compact extended, extended, jetted, and disturbed. We find that the merging cluster environment has a statistically significant, higher population proportion of disturbed (bent and head tail) sources, indicating that the merging environment can affect the morphology of cluster radio-AGN. We also investigate the number of AGN that are detected in the radio data only, and the number that are detected in both the radio and optical data in mergers and non-mergers. We find that the merging cluster environment has a higher population proportion of AGN that are identified only as radio-AGN compared to AGN that are identified as both radio and optical AGN. Overall, we find that the merging environment affects certain radio-AGN (disturbed and only radio identified AGN), but not all.

*Keywords:* Galaxy clusters (584) – Active galactic nuclei (16) – Radio active galactic nuclei (2134)

### 1. INTRODUCTION

It is now well established that dense environments such as galaxy clusters affect the properties and evolution of the galaxies within them (see references detailed

below). There are a variety of interactions between the galaxies, the intra-cluster medium (ICM; a diffuse, hot, ionized plasma that is gravitationally bound to the cluster), and the cluster potential that are possible and prevalent in clusters that affect properties and evolution of galaxies. Some examples of the possible interactions are galaxy-galaxy harassment (repeated close encounters with neighbors; Moore et al. 1996, 1999), galaxy-cluster potential tidal effects (Fujita 1998; Natarajan et al. 1998), and galaxy interactions with the ICM, such as ram pressure stripping (Gunn & Gott 1972)

Corresponding author: Emily Moravec  
emoravec@nrao.edu

\* co-first author

Mary Rickel was a summer student at Green Bank Observatory

† co-first author

and strangulation (Larson et al. 1980). These interactions can affect the star formation rates (Kauffmann et al. 2004; Fassbender et al. 2014; Barsanti et al. 2018), active galactic nuclei (AGN) activity (Galametz et al. 2009; Bufanda et al. 2017; Poggianti et al. 2017; Marshall et al. 2018; Mo et al. 2018), morphology (Dressler 1980; Kauffmann et al. 2004; Sazonova et al. 2020), and gas supply of the cluster galaxies (Stroe et al. 2015; Poggianti et al. 2017; Jaffé et al. 2018; Cairns et al. 2019).

One classic example of the effect of the cluster environment on its galaxies is the morphology–density relation, in which, with increasing density, the fraction of elliptical galaxies increases and the fraction of spiral galaxies, decreases such that clusters typically have an overabundance of elliptical galaxies compared to the field (Dressler 1980; Kodama et al. 2001; Kauffmann et al. 2004; Sazonova et al. 2020). Coupled to the morphology–density relation is the star formation rate, where more star-formation is seen in galaxies at low densities and less at high densities (Kauffmann et al. 2004; Fassbender et al. 2014). There is an evolution of these properties as a function of redshift, in that, with decreasing redshift, the fraction of “red and dead” galaxies increases (De Lucia et al. 2004; Rudnick et al. 2009) and the fraction of star forming galaxies decreases (Margoniner et al. 2001; Poggianti et al. 2006; Saintonge et al. 2008). Another example of the environment affecting cluster galaxies is the case of “jellyfish” galaxies, which are galaxies typically located near the cores of the clusters that are experiencing ram pressure stripping, leaving a tail of gas behind them opposite to the direction of motion (Fumagalli et al. 2014; Ebeling et al. 2014; Jaffé et al. 2018).

The cluster environment is also known to affect the properties and evolution of cluster galaxies that host AGN. AGN are powerful astrophysical sources that are fueled by accretion of matter onto the supermassive black hole at the center of the galaxy and emit characteristic radiation signatures across the full electromagnetic spectrum (Padovani et al. 2017). AGN can be identified in one or multiple wavelengths such as X-ray, optical, infrared, or radio. At all redshifts Galametz et al. (2009); Mo et al. (2018) find that there is an excess of radio identified AGN in clusters, and specifically at the center of clusters compared to the field, which is more pronounced at high redshift (Galametz et al. 2009; Mo et al. 2020). Similarly, pertaining to X-ray, optical, and infrared identified AGN, the number density of AGN continually increases as a function of redshift in that there is a deficit of these types of AGN near the cluster center at  $z \lesssim 0.5$  (Pimblet et al. 2013; Ehlert et al. 2014; Gordon et al. 2018), but at  $z \gtrsim 0.5$  there is an excess of these types of AGN in clusters (Ruderman &

Ebeling 2005; Galametz et al. 2009; Fassbender et al. 2012; Martini et al. 2013; Alberts et al. 2016; Bufanda et al. 2017) which is most pronounced near the cluster center (Ruderman & Ebeling 2005; Galametz et al. 2009; Fassbender et al. 2012; Alberts et al. 2016). The cluster environment seems to affect many different properties of radio-AGN in particular, such as the size, luminosity, and morphology of the radio-AGN (Prestage & Peacock 1988; Gendre et al. 2013; Ineson et al. 2015; Croston et al. 2019; Garon et al. 2019; Moravec et al. 2020; Maccioni et al. 2020; Shen et al. 2020; Morris et al. 2022). Further, bent-tail radio galaxies are a very well-known type of radio-AGN that showcase the effect of the environment on radio-AGN produced by the ram pressure of the dense environment (Miley et al. 1972; Begelman et al. 1979; O’Donoghue et al. 1993; Hardcastle et al. 2005; Morsony et al. 2013).

Galaxy clusters undergo cluster-cluster mergers (henceforth mergers<sup>1</sup>) as a result of hierarchical structure formation in the Universe (Voit 2005; Springel et al. 2005; Boylan-Kolchin et al. 2009; Klypin et al. 2011; Pillepich et al. 2018; Planck Collaboration et al. 2020). Mergers have an immense and obvious impact on the properties of the ICM. For example mergers cause the ICM distribution to be asymmetric seen by X-ray (Buote 2002) and Sunyaev–Zeldovich observations (Mroczkowski et al. 2019). Further, mergers drive intergalactic shocks and induce turbulence in the ICM (Sarazin 2002; Markevitch 2006; Basu et al. 2016). And lastly mergers can create cold fronts in the ICM (Sarazin 2002; Owers et al. 2009; Roediger et al. 2013) and disrupt the cool cores of clusters (Sarazin 2002).

Although the effect of mergers on the ICM is clear, the impact on the cluster galaxies is less so. There is contradictory evidence that mergers can either increase (Owen et al. 1999; Miller & Owen 2003; Hwang & Lee 2009) or decrease (Hwang & Lee 2009; Mansheim et al. 2017) star formation in cluster galaxies. One study found that a dynamically younger cluster had a higher fraction of galaxies with a high star formation rate ( $>0.17 M_{\odot} \text{ yr}^{-1}$ , Stroe et al. 2015). There is also evidence that a brief period of enhanced, triggered star formation may be followed by subsequent quenching (Stroe et al. 2015; Cairns et al. 2019). These results are attributed to a disturbed ICM affecting the molecular gas reservoir of the cluster galaxies, with the disturbance exciting star formation and leading to a rapid consumption of the molecular gas (Stroe et al. 2015; Cairns et al. 2019).

<sup>1</sup> In this work we refer to cluster-cluster mergers as “mergers” which we differentiate from the typical galaxy-galaxy mergers that many in the literature refer to as “mergers.”

Recent work has found that the AGN population is impacted by cluster-cluster mergers as well. The radio-AGN population in particular has been studied in depth in individual merging systems and found to have a higher frequency compared to The radio-AGN frequency in more relaxed systems (e.g., Miller & Owen 2003; Moravec et al. 2020). Similarly, Noordeh et al. (2020) found enhanced X-ray AGN activity in the most dynamically disturbed of the seven clusters they studied. Bilton et al. (2020) find that mergers hold relatively kinematically younger AGN sub-populations that have recently coalesced into a common potential (similar to a first infall population of galaxies) compared to relaxed clusters. In general, Miller & Owen (2003); Hwang & Lee (2009); Sobral et al. (2015) find that mergers can provoke AGN activity. However, the physical mechanism by which mergers instigate AGN activity and its effects on radio-AGN properties is unknown.

In this paper, we explore the effect of mergers on the morphology of radio-AGN. In §2, we explain the sample and data used in this work. In §3, we describe the methods used to create images of the radio-AGN and classify them. In §4, we present the results of our investigations into the morphology and number of radio-AGN in mergers versus non-mergers and compare them to optically identified AGN. In §5, we discuss the implications of our results and in §6 we summarize our findings. Throughout this paper we use a cosmology in which  $H_0 = 70 \text{ km s}^{-1} \text{ Mpc}^{-1}$ ,  $\Omega_m = 0.3$ , and  $\Omega_\Lambda = 0.7$ .

## 2. SAMPLE AND DATA

### 2.1. The SDSS Galaxy Cluster Sample

The parent sample of galaxy clusters used for this study was obtained from Bilton et al. (2020). This galaxy cluster sample was assembled with Sloan Digital Sky Survey Data Release 8 galaxies (SDSS DR8; York et al. 2000; Aihara et al. 2011), which were constrained by parameters found in the literature, and compiled into the X-Ray Cluster Database (BAX; Sadat et al. 2004). Where the SDSS DR8 spectroscopic data is magnitude limited in the r-band to  $m_r \lesssim 17.77$  (Strauss et al. 2002). Furthermore, the MPA-JHU value-added catalogue was cross-matched to the DR8 membership, in particular for their stellar mass estimates, in order to maintain completeness (Kauffmann et al. 2003; Brinchmann et al. 2004; Salim et al. 2007).

Bilton et al. (2020) used the BAX galaxy cluster database to constrain the initial galaxy cluster sample to an X-ray luminosity range  $1 < L_X \leq 20 \times 10^{44} \text{ erg s}^{-1}$ . Applying these limits ensures that the most mas-

sive, well-assembled galaxy clusters are selected, while maintaining a sufficiently sized sample that can represent varying dynamical states within the finite limits of the  $z$ -space that can be feasibly observed. After initial constraints were applied, the final cluster memberships for each cluster were then produced through surface caustics from the mass estimation methods of Diaferio & Geller (1997) and Diaferio (1999). These surface caustics vary as a function of projected radius  $R$  from the cluster centre, thereby leading to the finalized membership being found within the confines of these caustics (see Gifford & Miller 2013; Gifford et al. 2013). Once the cluster galaxy membership had been ascertained, Bilton et al. (2020) proceeded to distinguish between relaxed and unrelaxed states, or ‘non-merging’ and ‘merging’ respectively. This was achieved via the incorporation of the Dressler & Shectman (1988) statistical test for substructure (also known as the  $\Delta$ -test), where the presence of substructure is used as a proxy for a galaxy cluster in a ‘merging’ or unrelaxed dynamical state. The details of this statistical test and its calculation are elaborated on in Bilton et al. (2020).

Utilising the DR8 spectral lines for  $H\alpha$  and [NII]  $\lambda 6584$ , so-called ‘WHAN’ diagrams can be used as a diagnostic to determine whether a cluster galaxy hosts an AGN or not (Cid Fernandes et al. 2010, 2011). Specifically, the equivalent width of  $H\alpha$ ,  $EW_{H\alpha}$ , is compared to the logarithmic ratio of  $\log_{10}([\text{NII}]/H\alpha)$ . The reduction of the number of emission lines for a WHAN diagram to two allows for mitigation against the  $\text{SNR} \geq 3$  requirements for all emission lines, especially when compared to the Baldwin-Philips-Terlavič (BPT) diagnostic plot’s use of four emission lines (Baldwin et al. 1981). We refer to these WHAN selected AGN as optical AGN in the rest of this work. Furthermore, to reduce the number of interloping star-forming galaxies and Low Ionisation Emission Regions (LIERs), galaxies are classified as AGN if they possess emission ratios and strengths of  $\log_{10}([\text{NII}]/H\alpha) \geq -0.32$  and  $EW_{H\alpha} \geq 6 \text{ \AA}$  respectively.

During our initial analysis of the cluster member catalogs from Bilton et al. (2020), we discovered duplicate sources. We determined that these duplicates were a product of the fact that the SDSS DR8 spectroscopic catalog contains multiple measurements for some sources (along the plate overlap regions). We removed the 143 duplicate sources, which leaves us with a total of 2,298 objects.

In addition to the duplicates found within each cluster, we also found 42 sources that were counted as members in both the Abell 2029 and Abell 2033 member catalogs. We note that Walker et al. (2012) show X-ray evidence of overlap between these two systems. To remedy this,

**Table 1.** Galaxy clusters studied in this work

| Cluster    | R.A.<br>(J2000) | Dec.<br>(J2000) | $z$   | $N$ | RMS<br>(mJy beam <sup>-1</sup> ) | $D_{\text{state}}$ |
|------------|-----------------|-----------------|-------|-----|----------------------------------|--------------------|
| Abell 1367 | 11:44:29.5      | +19:50:20.6     | 0.022 | 58  | 0.245                            | NM                 |
| Abell 1656 | 12:59:48.7      | +27:58:50.5     | 0.023 | 96  | 0.117                            | NM                 |
| Abell 1795 | 13:49:00.5      | +26:35:06.8     | 0.062 | 46  | 0.127                            | NM                 |
| Abell 2029 | 15:10:56.0      | +05:44:41.0     | 0.077 | 98  | 0.307                            | NM                 |
| Abell 2061 | 15:21:15.3      | +30:39:16.7     | 0.078 | 95  | 0.0913                           | NM                 |
| Abell 2065 | 15:22:42.6      | +27:43:21.5     | 0.073 | 87  | 0.123                            | NM                 |
| Abell 2069 | 15:23:57.9      | +29:53:25.8     | 0.116 | 57  | 0.0765                           | NM                 |
| Abell 2199 | 16:28:38.5      | +39:33:06.0     | 0.030 | 120 | 0.16                             | NM                 |
| Abell 2255 | 17:12:31.0      | +64:05:33.3     | 0.081 | 83  | 0.18                             | M                  |
| Abell 1991 | 14:54:30.2      | +18:37:51.1     | 0.044 | 63  | 0.116                            | M                  |
| Abell 2033 | 15:11:28.1      | +06:21:43.7     | 0.082 | 41  | 0.184                            | M                  |
| Abell 426  | 03:18:36.4      | +41:30:54.2     | 0.018 | 64  | 0.269                            | M                  |

NOTE—Sample of clusters used in this analysis. Cluster name, coordinates, redshift ( $z$ ), number of cluster members ( $N$ ) identified by optical SDSS data in [Bilton et al. \(2020\)](#), global RMS value of LoTSS image (mJy beam<sup>-1</sup>), and dynamical state ( $D_{\text{state}}$ ), merging or non-merging, for clusters from [Bilton et al. \(2020\)](#) covered by LoTSS.

for each of these 42 duplicate members we calculate a statistic,  $C$ , which is based on both projected separation and relative velocity ([Smith et al. 2004](#)). The statistic  $C$  is defined as

$$C = (cz - cz_{\text{cl}})^2 / \sigma_{\text{cl}}^2 - 4 \log(1 - R/R_{\text{cl}}) \quad (1)$$

where  $c$  is the speed of light,  $z$  is the redshift of the galaxy,  $z_{\text{cl}}$  is the cluster redshift,  $\sigma_{\text{cl}}$  is the velocity dispersion of the cluster,  $R$  is the projected radius of the galaxy from the cluster center in  $r_{200}$ , and  $R_{\text{cl}}$  is the radius of the cluster in units of  $r_{200}$ . We then assign the member to the cluster that minimizes  $C$  ([Smith et al. 2004](#)). Minimizing  $C$ , 37 of the duplicates are assigned to Abell 2029 and 5 assigned to Abell 2033.

## 2.2. LoTSS Data

To examine the radio characteristics of the cluster members, we used data from the LOFAR Two-metre Sky Survey (LoTSS: [Shimwell et al. 2017](#)). LoTSS provides a resolution of 6'' with a central frequency of 144 MHz and a median RMS sensitivity in public data of 83  $\mu\text{Jy}/\text{beam}$ . We made use of the current public data release of LoTSS which is Data Release 2 ([Shimwell et al. 2022](#)), and in addition we made use of data processed since that release, which will be made publicly available in LoTSS Data Release 3.

Out of the 33 clusters from [Bilton et al. \(2020\)](#), 13 were covered by the LoTSS survey, 9 non-merging and

4 merging. Of these 13 clusters, one cluster, Abell 119, was only half covered by the Sloan Digital Sky Survey and was therefore discarded from the analysis. As a result, our final sample consisted of 12 clusters fully covered by LoTSS and SDSS (see Table 1). For each of these clusters we made a mosaiced image which combined all of the available LoTSS pointings covering that cluster, maximizing the sensitivity of the images used for this study.

## 2.3. Completeness and Redshift Distribution

It is known that SDSS completeness drops to  $\approx 65\%$  in denser fields such as a galaxy cluster ([Yoon et al. 2008](#)) due to there being more targets than available fibers. To investigate the completeness of our sample, we compare the average mass of the galaxy clusters and number of cluster members across both dynamical states. When examining the [Bilton et al. \(2020\)](#) SDSS catalogs of the LoTSS covered clusters, we find an average 62 members per merging cluster and 82 per non-merging cluster. When we match these averages with average cluster halo mass, we find mergers have  $5.4 \times 10^{14} M_{\odot}$  and non-mergers  $6.3 \times 10^{14} M_{\odot}$ . Cluster mass,  $M_{200}$ , is determined in [Bilton et al. \(2020\)](#) from the density profile  $\rho(r) = 3M(r)/4\pi r^3$ , where  $\rho(r)$  is specifically 200 times the critical density of the flat Universe. If we compare the number of cluster members and halo masses of the

clusters, we find merging clusters relative to non-mergers have about 75% of the members and 80% of the mass. The similarity of these values is suggestive that there’s not a significant selection bias.

In addition to survey completeness, we investigate the redshift distribution within each merging and non-merging populations to ensure that they are well-matched. Given this work is rooted in morphology, there exists a potential bias of a morphology class being mistaken for another due to resolution issues coming from redshift differences. For the non-mergers, we find the mean  $z$ , median  $z$ , and interquartile range to be 0.06, 0.07, and 0.05. For mergers, we find the mean  $z$ , median  $z$ , and interquartile range to be 0.06, 0.06, and 0.05. The redshifts are well matched between the cluster dynamical state populations and we do not expect redshift to bias morphological classifications within each population.

### 3. METHODS

In order to determine whether or not the merging cluster environment affects the radio morphology of AGN and cluster galaxies, the radio sources need to be classified according to their morphology. To do this, we created images (§3.1), devised a classification system (§3.2), visually inspected the radio sources (§3.3), and determined which sources were radio-AGNs (§3.5).

#### 3.1. Cutouts

In preparation for classification, we needed to create cutouts of each source with radio emission. To do this, we first obtained LoTSS images of each cluster that were  $2 r_{200} \times 2 r_{200}$ . Once the images were obtained, we made “cutouts” or images that were zoomed in on each cluster member. The dimensions of these cutouts varied in size from  $12'' \times 12''$  for compact emission to  $60'' \times 60''$  in order to be able to showcase the extended emission of the source.

Since there were a large number of sources and respective cutouts to be made, there was a necessity to be able to create bulk cutouts for the classification process. Thus we calculated and used a “global” cluster noise (henceforth referred to as RMS or  $\sigma$ ) for generating contours for the radio sources. To determine the global RMS for each LoTSS image, we made use of SAOImageDS9 (Joye & Mandel 2003). For each mosaiced cluster image, we selected an emission-free region and drew a circle  $\approx 4$  arcminutes in diameter within this region. From this circle, we extracted the RMS in mJy beam $^{-1}$  from the statistics calculated automatically in DS9. For each cluster, we used this global cluster RMS to produce the contours for the cluster member cutouts (reported in Table 1).

The method of calculating the RMS and contour levels displayed for the cutouts can influence the appearance and thus the morphology classification of the source. Given our dataset, which comprises over 1000 sources, we were confronted with a trade-off between efficiency and sensitivity. We investigate whether the morphology classification of a source is RMS (and corresponding contour levels) dependent by selecting a handful of sources (14) showing faint emission potentially related to the source but not captured with contours and testing the effect of using different RMS values. For these sources, we created new cutouts using varying RMS and contour levels. We compared the original, global RMS and contour level for each image to 1) the local RMS (determined from a  $r = 100''$  circle of an emission free region in the cutout) with the original  $4\sigma \times 2^n$  base for contours, 2) the original global (cluster) RMS but with a 3, 4, 5,  $8\sigma$  contour levels, and 3) the local RMS with 3, 4, 5,  $8\sigma$  contour levels. We find no significant deviation from the original classification results when comparing the new RMS and contour levels. As a result, we are confident that our choice of using a global RMS is robust.

To aid with the classification process, we displayed contours in the cutouts that were log-based starting with a  $4\sigma$  base determined by the cluster RMS, as described above. Thus, the contours begin with  $4\sigma$  and increase by factors of  $2^n$  where  $n = 1, 2, 3$ , etc. To optimize visualization for many hundreds of images, we employed a square root scaling technique in `aplpy` and scaled the images as a percentage of the maximum pixel value (`pmax=100`). To see all of these parameters in use see Figure 1.

#### 3.2. Radio Morphology Classifications

After the cutouts were made, one team member visually categorized the sources as having a radio detection or non-detection. A source was defined as having a radio detection if it had  $\geq 8\sigma$  detection at the cluster member coordinate from the Bilton et al. (2020) catalog, which manifested visually as two contours (at a  $4\sigma$  base). We chose  $8\sigma$  as the threshold for a detection for the following reasoning. Because we used a global, cluster RMS to create the contours for the cluster members, there are a few cases where  $4\sigma$  contour encapsulates the noise instead of the morphology of the source, making the radio morphology of the source difficult to classify. Since we were classifying the sources as detection or non-detection visually (to be consistent with the visual radio morphology classification), we increased the base of detection to the next displayed contour which in this case is  $8\sigma$  (because we define the contours as  $4\sigma \times 2^n$  where  $n$

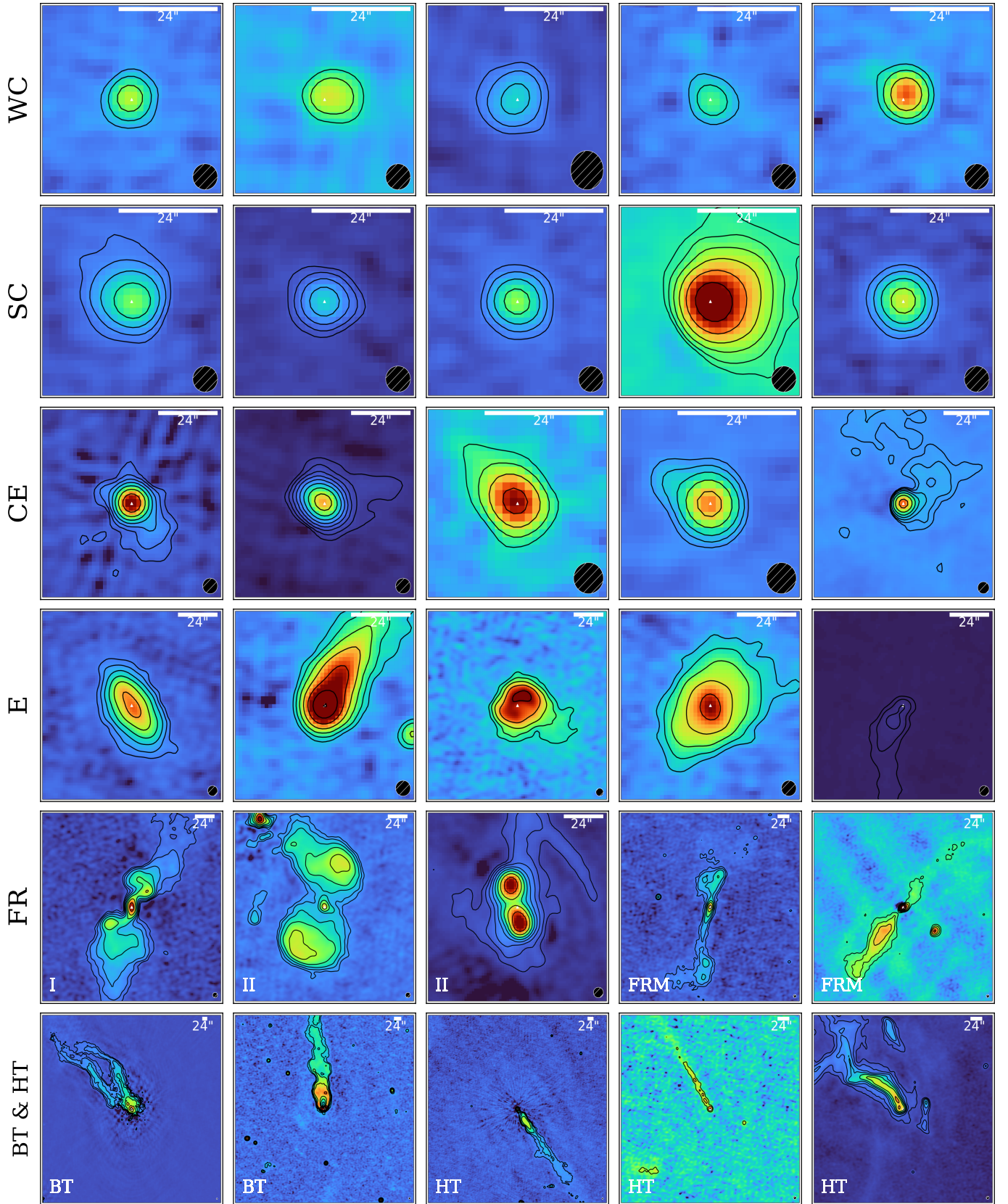


**Figure 1.** Examples of all classifications. See §3.2 for classification definitions. Representative images use the local RMS (determined from a  $r = 100''$  circle of an emission free region in the cutout) with the original  $4\sigma \times 2''$  base for contour level. These images may differ slightly from those shown to classifiers. For all, the LoTSS beam is displayed in the lower right-hand corner.

= 0, 1, 2, etc.) in order to be confident that the contours were displaying radio emission and not noise.

After visual inspection of the cutouts of the [Bilton et al. \(2020\)](#) sample of 2,298 galaxies (1670 from non-mergers, 628 from mergers), we find that 191 had a radio detection. These radio detection images were uploaded to Zooniverse<sup>2</sup> for visual morphological classification by five team members (M.R., E.M., Y.A.G., L.E.B., J.C.S.P.).

Creating a classification scheme was an iterative process. There was an initial, baseline classification scheme that was created during preliminary work based on the spatial distribution, extension, and strength of the radio emission of the source. After testing this initial classification scheme, we converged on a final morphology scheme that we used on Zooniverse and is as follows (in order of increasing level of disturbance):

- **Weak Compact (WC):** Emission is (a) roughly circular, (b) on a scale of less than or roughly equal to 12" (2 times the resolution of LoTSS), and (c) has 2 or 3 contours (8-16 $\sigma$  detection).
- **Strong Compact (SC):** Emission that is (a) roughly circular, (b) on a scale of less than or roughly equal to 12" (2 times the resolution of LoTSS), and (c) has 4 or more contours ( $\geq 32 \sigma$  detection). There may be sources that have 4 contours and are roughly circular but are larger than 12" (up to 30" in size); these are still strong compact<sup>3</sup>.
- **Compact Extended (CE):** Emission has a compact (roughly circular and with a size of less than or roughly equal to 30") core with a singular source of extended emission that is on the order of or greater than 12" (2 times the resolution of LoTSS).
- **Fanaroff and Riley Type I (FRI):** A source that follows the canonical FR I type morphology ([Fanaroff & Riley 1974](#)) and is not bent.
- **Fanaroff and Riley Type II (FRII):** A source that follows the canonical FR II type morphology ([Fanaroff & Riley 1974](#)) and is not bent.
- **Fanaroff and Riley Type Morphology (FRM):** A source with clear two-sided non-bent jets, but FR classification is unclear.
- **Extended (E):** Emission that is (a) clearly on a much larger scale than that of the compact sources on the order of or much greater than 5 times the resolution of LoTSS (30") but is not an FRI, FRII, Bent Tail, or Head Tail source and (b) is irregular in shape (not circular).
- **Bent Tail (BT):** A source in which the jets are bent to some degree. Either or both jets could be slightly or extremely bent.
- **Head Tail (HT):** An extreme bent tail source where the two jets/tails are indistinguishable
- **Undetermined<sup>4</sup>:** There is obviously a source in the anticipated location but the classification is uncertain.
- **Bad Data:** When there are clearly imaging artifacts interfering with the source.
- **No Detection:** Those that have no emission near the position of the cluster member (indicated by a triangle).

Sources are classified as Undetermined if their morphology does not follow the definition of any provided classifications. The classification system describes the majority of our sample. We note that no morphological classification scheme will be able to exhaustively describe all of the possible complex morphologies. Exemplary sources of each classification are shown in Figure 1.

### 3.3. Zooniverse Project

To obtain robust classifications, five team members visually classified each source. For image sharing and collaborative classification, we made use of the Zooniverse Website, a platform, a widely recognized online tool designed for projects reliant on classification-based tasks ([Lintott et al. 2008](#)). We established a private project and invited collaborators who are experts in fields relating to the scientific scope of this paper to participate. Upon joining the project, each classifier was presented with a randomly selected radio image from the dataset and prompted to classify it based on the classification criteria described in 3.2. The classifiers were blind to the dynamical state of the parent cluster (merging vs. non-merging) and to which cluster each source came from. The accumulated results from these five evaluators were

<sup>2</sup> [Zooniverse website](#)

<sup>3</sup> This condition is meant to catch strong compact sources that only differ from the original classification by being larger than 2 times the LoTSS resolution.

<sup>4</sup> In the Zooniverse project this classification was called "Uncertain" but the name of the classification was changed to Undetermined for the written to avoid confusion with other types of uncertainty. The change in classification class name does not change any results.

incorporated into this study for analysis. We note that each classifier was allowed to give each source at most one radio classification and multiple classifications were not allowed.

### 3.4. Consensus level

We aggregate the votes from Zooniverse. Following the aggregation of votes from Zooniverse, we define multiple levels of consensus. Consensus level was determined by the number of classifiers (of the 5 total) that agreed on a source classification. For example, in order to create a group of sources for which we were extremely confident in their classification, we define “consensus level 4” as 4 or 5 out of 5 classifiers agreed on a classification. Next, to retain a majority classification but include as many sources as possible, we define “consensus level 3” as 3 of the 5 classifiers agreed on a classification. Consensus level 3 also includes classifications that had a consensus level of 4. Lastly, we define a “non-consensus” class where 2 or fewer classifiers agreed on a classification. There are 71 consensus level 5 sources, 120 consensus level 4 sources, 166 consensus level 3 sources, and 25 non-consensus sources.

We find that the results in this work remain consistent when using consensus level 3 or 4. A comparison between these two consensus levels is described in Appendix B. Because the overall trends are the same in both samples, we use the consensus level of 3 to serve as the standard consensus level for the analysis in this work.

There were 9 sources out of the total 166 consensus level 3 sources that were removed from the sample. There were 6 poor-image-quality sources that were removed. Any sources that appeared to have significant artifact contamination or very low strength as compared to the background image, were classified as bad data (1) or no detection (5) respectively and removed. Additionally, we omit the single source classified as undetermined in the consensus level 3 sample as we want to investigate sources with a distinct radio morphology. We omit these sources (7) from the analysis for a total of 159 consensus level 3 sources. However, for the sake of completeness, we note here that after the radio-AGN delineation process we removed two Extended sources (the reason for which is discussed at length at the end of Section 3.5) for a total of 157 sources. We refer to these sources as the “Zooniverse results” and provide a catalog of these 157 sources with this work for download and display the first 20 rows of this catalog in Table 4.

### 3.5. AGN vs. Star Forming in Compact Radio Morphologies

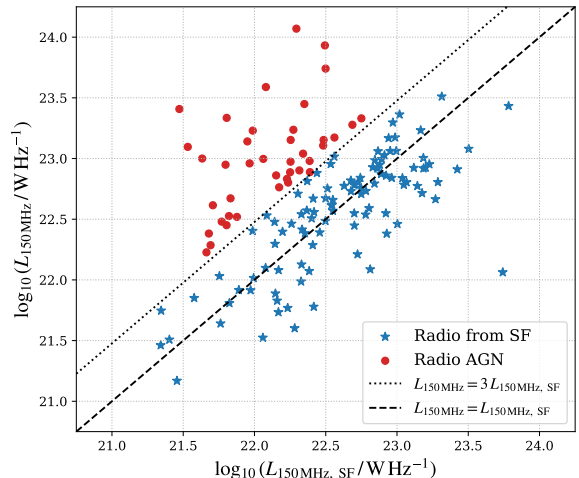


**Figure 2.** Expected radio emission due to star-formation,  $L_{150 \text{ MHz, SF}}$ , versus 150 MHz for our compact radio sources. The black dashed line shows where the measured luminosity is equal to the luminosity expected due to star-formation, while the dotted line shows  $L_{150 \text{ MHz}} = 3 L_{150 \text{ MHz, SF}}$  that we use to identify sources where the radio emission is due to an AGN (red circles) as opposed to possibly being the result of star-formation (blue stars).

We further filter the 159 Zooniverse consensus 3 level sources from §3.4 to only those that are radio-AGN in the following way. For radio galaxies with jetted and disturbed morphologies (11 total from the FR I, FR II, FRM, HT, and BT categories) it is clear that the radio emission is the result of an AGN. However, for compact radio sources where the AGN jet is unresolved, we must consider another possibility for the radio emission. In galaxies that do not host an AGN, star-formation produces radio emission, primarily as the result of synchrotron emission from supernovae shocks and thermal emission from H II regions (Condon 1992). Generally, radio emission from star-formation is relatively low luminosity, dominating the local radio luminosity function at  $L_{1.4 \text{ GHz}} < 10^{23} \text{ W Hz}^{-1}$  (Best et al. 2005). In order to analyse the impact of the cluster environment on radio-AGN, it is therefore important to establish that the radio emission for compact objects is indeed the result of an AGN and not star-formation.

For the simple-morphology radio sources in our sample, namely those classified as WC, SC, or CE (141 sources), we estimate the expected 150 MHz emission due to star-formation based on their measured SFRs using the relation of Gürkan et al. (2018). For these sources the 150 MHz flux density is measured from the LoTSS images using Mohan & Rafferty’s PyBDSF (Mohan & Rafferty 2015). Additionally, the galax-



ies in our sample are in the SDSS DR8 spectroscopic catalog and have star-formation rate (SFR) measurements from the MPA-JHU catalog (Brinchmann et al. 2004). By comparing the measured radio luminosity,  $L_{150\text{ MHz}}$ , to the radio luminosity expected from star-formation,  $L_{150\text{ MHz, SF}}$ , we can thus identify the likely source of the radio emission in our galaxies (see Figure 2). The Gürkan et al. (2018) relation between SFR and radio luminosity has a typical uncertainty of 1.68. To account for this, and given that we are looking to only include radio-AGN in our analysis, we adopt a conservative approach and consider sources with  $L_{150\text{ MHz}} > 3 L_{150\text{ MHz, SF}}$  as radio-AGN (red circles on Figure 2). We find that 103 of our simple morphology radio sources have radio emission that can be explained by star formation, leaving us with 38 radio-AGN in our sample that have WC, SC, or CE morphologies.

Further, of the seven E morphologies, three were easily delineated as radio-AGN or star forming using the flux cutoff from their LoTSS catalog value. Two sources are visually determined to possess a degree of jetting on this second pass and therefore are classified as radio-AGN. We honor the original classification of E for these sources, as poorly resolved jetted sources classified as E is a possible uncertainty discussed later in Section 4.1. Of the remaining two E sources, one did not have a LoTSS catalog entry and could not be detected by Mohan & Rafferty’s PyBDSF. Because this source does not a reliable flux measurement and cannot be placed on the Gürkan et al. (2018) relation, we exclude this source. Through optical counterpart analysis, the last E source appears to be the overlap of two spiral galaxies but with only one LoTSS entry. Because it is not possible to determine which galaxy is contributing to the radio emission, we also drop this source from the analysis. Since these two sources were not able to be classified as a radio-AGN or not, we entirely remove them from the sample, reducing the sample from 159 sources to 157 sources.

Using this analysis to separate out the radio-AGN, we find that 43 sources are radio-AGN that have WC, SC, CE or E morphologies in consensus level 3. Thus, as a result, from the 157 Zooniverse sources, the final sample of sources that we use for analysis in the following work is 54 radio-AGN consensus level 3 sources (11 FR I, FR II, FRM, HT, or BT + 43 WC, SC, CE or E).

While ram pressure stripping can boost the radio luminosity of a source, this is most extreme (approximately a factor of 3) at  $L_{144} < 10^{21}$  W/Hz, with much lower levels of radio luminosity boosting at  $L_{144} < 10^{22}$  W/Hz (see Figure 9 of Roberts et al. 2021). All of our selected radio galaxies have  $L_{144} < 10^{22}$  W/Hz and thus

subject to low levels of radio luminosity boosting by RPS. Furthermore, our radio galaxy sample are chosen to have radio luminosities of at least 3 times the expected radio luminosity due to SF (see Fig. 2). As such we are confident that all of our selected radio galaxies host a radio-loud AGN.

### 3.6. Statistical Methods

We want to compare the proportion of observed radio morphology classes in mergers and non-mergers within the uncertainties. To do this, we express our results as proportions ( $P = k/n$ ), where  $k$  is the number of radio-AGN of a particular radio morphology in mergers or non-mergers and  $n$  is the total number of radio sources for the respective dynamical state.

Given the small number statistics and asymmetric errors on the proportions measured, care is necessary in quoting and defining uncertainties. We take a Bayesian approach and give credible intervals on the true proportion  $P$  given the observed  $k$  and  $n$ . For a Jeffreys prior, the posterior probability distribution of  $P$  is a Beta distribution:

$$p(P|k, n) = \text{Beta}(k + \frac{1}{2}, n - k + \frac{1}{2})$$

and hence the credible interval can be taken to be the relevant percentile of the Beta distribution (e.g. 16 and 84% for a  $1\sigma$  range as used here). It is conventional to set the lower range to 0 if  $k = 0$  and the upper range to 1 if  $k = n$  (the Jeffreys interval, which is indicated as the lower and upper uncertainties on Figure 3), as implemented in the ASTROPY.STATS function BINOM\_CONF\_INTERVAL.

It is important to note that, given the asymmetric nature of these errors and the fact that the posterior distribution about  $k/n$  is far from being a Gaussian, it is not possible simply to combine the quoted ‘errors’ (credible interval) in order to compare two different proportions with one another, or to multiply by a constant to get a  $3\sigma$  confidence range. If we observe two proportions  $P_1(k_1, n_1)$  and  $P_2(k_2, n_2)$  where  $k_1/n_1 < k_2/n_2$ , then the Bayesian way of asking the question ‘is  $P_2$  significantly greater than  $P_1$ ’ is ‘is there a high posterior probability that  $P_2 - P_1 > 0$ ?’ This could be found exactly by convolving the two posterior distribution functions, but for simplicity we simply subtract samples drawn from  $P_1$  and  $P_2$ , which allows us to estimate this posterior probability to adequate precision (listed as  $\text{Pr}(M > NM)$  in Table 2). We map the  $\text{Pr}(M > NM)$  to a statistical significance level using a one-tailed test by inverting the cumulative distribution function of a Gaussian. Although an approach framed as ‘is there a difference?’ or in other words testing if  $\text{Pr}(M > NM)$  or  $\text{Pr}(M < NM)$ , may seem

less biased, there are cases where the proportion is 0, making it unreasonable to test for any direction other than greater. For consistency, we maintain a one-tailed approach throughout the analysis. These statistical significances are quoted and interpreted in Section 4.1, taking the standard approach that 68%, 95%, and 99.7% correspond to  $1\sigma$ ,  $2\sigma$ , and  $3\sigma$ , respectively.

#### 4. RESULTS

After determining consensus and radio-AGN delimitation, we analyze the trends in our data based on morphology (see §4.1) and AGN classification (see §4.2).

##### 4.1. Combined Classifications and Results

Though the individual classifications defined in §3.2 trace unique behavior across sources, we establish combined classification groups to trace general radio morphology classification trends between the cluster dynamical states. We define the following combined radio morphology classification groups based on morphological similarity:

- **Compact:** This group of classifications combines the sources that are physically compact: weak compact (WC) and strong compact (SC) sources. The sources are grouped together because they fundamentally share the same characteristic in terms of scale of emission, only differing in emission strength.
- **Compact Extended:** This group of classifications includes only compact extended (CE) sources. We keep CE separate from the compact objects as they exhibit a single extension, but differ from clearly extended, as they have a clear compact core.
- **Extended:** This group includes only the sources in the extended (E) category. In this sample, sources categorized as extended possess a great range in morphology.
- **Jetted:** This group combines sources that have FR I, FR II, or FRM classifications. First, we combine these classes in order to increase the number of sources in this class and second, because they both display unbent jets that have clear two-sided jet morphology. It is not important to distinguish between FR I and FR II for this work because they both have unbent, two-sided jets which are similar morphologically compared to the other types of morphologies considered in this work (e.g., compact, bent, etc.)

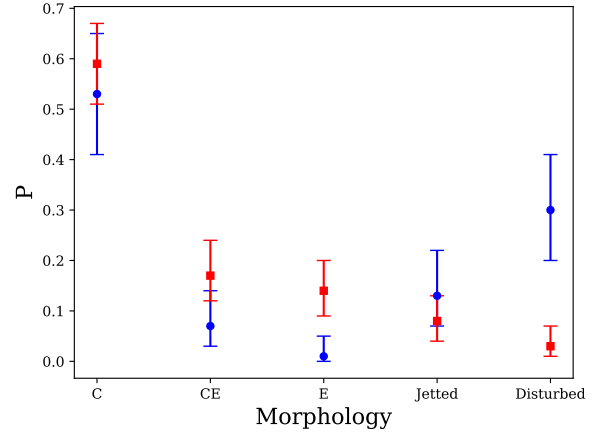


**Figure 3.** Binomial proportions ( $P$ ) for all combined classifications visualized for non-mergers (red squares) and mergers (blue circles) referenced in Table 2. Upper and lower bound uncertainties are the 86th and 16th percentile value, respectively, from the beta-binomial distribution described in Section 3.6.

- **Disturbed:** This group of classifications combines Bent Tail (BT) and Head Tail (HT) sources. Tailed sources are indicative of ram pressure stripping as a galaxy navigates the dense ICM. The degree to which a source is bent is beyond the scope of this work, thus we simply combine all sources that have jets that are bent to some degree to differentiate the bent from unbent radio morphologies.

Enumerated in Table 2 and visually in Figure 3, we report the proportion and uncertainties (described in §3.6) of the combined morphology classifications. In non-mergers, we observe a population proportions of  $0.59^{+0.08}_{-0.08}$  compared to  $0.53^{+0.12}_{-0.12}$  in mergers. Similarly in the CE category, in non-mergers, the value is  $0.16^{+0.07}_{-0.05}$  compared to  $0.06^{+0.07}_{-0.04}$  in mergers. Using the posterior probabilities of the C and CE across mergers and non-mergers, the merging population does not exhibit statistically significantly greater proportions of either C and CE sources compared to non-mergers (in other words  $\sigma < 1$ ). The  $\sigma$  calculation follows from mapping  $\Pr(M > NM)$ , where  $\Pr(M > NM)$  is equivalent to  $(M - NM > 0)$  divided by  $N$  samples, to the corresponding  $\sigma$  values discussed in Section 3.6.

Interestingly, we find extended (E) sources only in non-mergers. In non-mergers, there is a population proportion of  $0.14^{+0.06}_{-0.06}$  compared to  $0^{+0.04}_{-0.04}$  in mergers. Mergers do not display a significantly greater ( $\sigma < 1$ ) population proportion of E sources as compared to the non-mergers. Sources classified as E range greatly in morphology. This classification aimed to describe all

**Table 2.** Radio-AGN morphology results for combined morphology classes.

|                   | C                                      | CE                                     | E                                      | Jetted                                 | Disturbed                              |
|-------------------|--|--|--|--|--|
| Tot <sub>NM</sub> | 22                                     | 6                                      | 5                                      | 3                                      | 1                                      |
| Tot <sub>M</sub>  | 9                                      | 1                                      | 0                                      | 2                                      | 5                                      |
| P <sub>NM</sub>   | 0.59 <sup>+0.08</sup> <sub>-0.08</sub> | 0.16 <sup>+0.07</sup> <sub>-0.05</sub> | 0.14 <sup>+0.06</sup> <sub>-0.05</sub> | 0.08 <sup>+0.05</sup> <sub>-0.04</sub> | 0.03 <sup>+0.04</sup> <sub>-0.02</sub> |
| P <sub>M</sub>    | 0.53 <sup>+0.12</sup> <sub>-0.12</sub> | 0.06 <sup>+0.07</sup> <sub>-0.04</sub> | 0 <sup>+0.04</sup>                     | 0.12 <sup>+0.09</sup> <sub>-0.06</sub> | 0.29 <sup>+0.11</sup> <sub>-0.10</sub> |
| Pr(M > NM)        | 0.325                                  | 0.146                                  | 0.039                                  | 0.68                                   | 0.998                                  |

NOTE—Column headers are shorthand for the combined classification groups: Compact (WC+SC), Compact Extended, Extended, Jetted (FRI+FRII+FRM), and Disturbed (HT+BT). Rows describe the total radio-AGN and proportion of the classification within non-mergers and mergers using a beta-binomial Jeffreys Bayesian prior to determine the upper and lower bound uncertainty. Pr(M > NM) corresponds to the posterior probability that a specific classification is greater in mergers compared to non-mergers, discussed in Section 3.6.

extended, amorphous emissions that could not be unambiguously classified as compact or jetted. Based on a preliminary, quick optical counterpart examinations by eye, E sources may arise from a variety of physical mechanisms including but not limited to starburst face-on spirals, jellyfish galaxies, and cluster member mergers. The physical reasoning for heightened E sources in non-mergers is unclear, and a more detailed follow-up with optical counterparts would pose an interesting future direction. The origin of the emission mechanism for E sources is beyond the scope of this paper and requires a multi-wavelength approach for robust analysis.

We find that the proportion of jetted sources in mergers is not significantly ( $1\sigma$ ) greater than the proportion of jetted sources in non-mergers. We find the observed population proportion to be  $0.12^{+0.09}_{-0.06}$  for mergers and non-mergers to be  $0.08^{+0.05}_{-0.04}$ . The jetted sources encompass all clear FR-type morphologies.

Lastly, we find that the merging systems have a greater proportion of disturbed sources than non-mergers, within the error. We find that mergers and non-mergers have a population proportion of  $0.29^{+0.11}_{-0.10}$  and  $0.03^{+0.04}_{-0.02}$ , respectively. Mergers observe a greater proportion of disturbed sources as compared to non-mergers, at the  $3\sigma$  level. In other words, we find the posterior probability that Pr(M>NM) is greater than the  $3\sigma$  equivalent probability of 0.997. After visually re-examining the images of the disturbed sources, we find that they appear to be both bent and head tails which are jetted sources that have been affected by ram pressure ( $P_{\text{ram}} = \rho v^2$ ) causing the jets to become bent to some degree (Miley et al. 1972; Owen & Rudnick 1976; Begelman et al. 1979; O’Dea & Owen 1985).

In summary, we find mergers do not exhibit greater proportions of C sources, CE sources, and Jetted sources while they contain no E sources and significantly more disturbed sources when compared to the non-mergers. Non-mergers have comparable proportions of C sources,

CE sources, Jetted sources, and contain all the E sources and significantly fewer disturbed sources as compared to the mergers. We believe that this is a result of the large-scale bulk motions of the ICM that are present in the merging environment (see discussion in §5).

#### 4.2. Comparing Radio and Optical AGN

In Table 3, we report the statistics of radio-AGNs that are (a) also identified as an optical AGN ( $\text{AGN}_{\text{Rad-Opt}}$ ) and (b) only identified in the radio ( $\text{AGN}_{\text{Rad}}$ ) across both dynamical states. For the  $\text{AGN}_{\text{Rad-Opt}}$ , we cross-reference our radio-AGN sources with the Bilton et al. (2020) optical AGN catalog and the sources that are in both samples are counted as  $\text{AGN}_{\text{Rad-Opt}}$ . Conversely, the radio-AGN in our sample that are not identified by Bilton et al. (2020) as an optical AGN and are classified as radio-AGN only and are thus counted as  $\text{AGN}_{\text{Rad}}$ .

In comparing the proportions of  $\text{AGN}_{\text{Rad-Opt}}$  and  $\text{AGN}_{\text{Rad}}$  in mergers and non-mergers, we only find one marginally significant result: there are more  $\text{AGN}_{\text{Rad}}$  than  $\text{AGN}_{\text{Rad-Opt}}$  in merging systems taking into account the errors at a  $2\sigma$  level. In other words, the posterior probability that Pr( $\text{AGN}_{\text{Rad}} > \text{AGN}_{\text{Rad-Opt}}$ ) within mergers is 0.96. Less significant but noteworthy, we find mergers exhibit a marginally greater proportion of  $\text{AGN}_{\text{Rad}}$  at the  $1.5\sigma$  level as compared to non-mergers, or the posterior probability that Pr(M>NM) is 0.86. Next, comparison of  $\text{AGN}_{\text{Rad}}$  and  $\text{AGN}_{\text{Rad-Opt}}$  proportions within non-mergers yield a Pr( $\text{AGN}_{\text{Rad}} > \text{AGN}_{\text{Rad-Opt}}$ ) equivalent statistical significance less than one, where the Pr( $\text{AGN}_{\text{Rad}} > \text{AGN}_{\text{Rad-Opt}}$ ) is 0.59. Lastly, the comparison of  $\text{AGN}_{\text{Rad}}$  and  $\text{AGN}_{\text{Rad-Opt}}$  across mergers and non-mergers, yield a Pr(M>NM) equivalent statistical significance of less than one, where Pr(M>NM) is 0.14.

## 5. DISCUSSION

**Table 3.** Distribution of optical and radio AGN across cluster dynamical states.

|                   | AGN <sub>Rad-Opt</sub>                 | AGN <sub>Rad</sub>                     |
|-------------------|--|--|
| Tot <sub>NM</sub> | 19                                     | 18                                     |
| Tot <sub>M</sub>  | 6                                      | 11                                     |
| P <sub>NM</sub>   | 0.51 <sup>+0.08</sup> <sub>-0.08</sub> | 0.49 <sup>+0.08</sup> <sub>-0.08</sub> |
| P <sub>M</sub>    | 0.35 <sup>+0.12</sup> <sub>-0.11</sub> | 0.65 <sup>+0.11</sup> <sub>-0.12</sub> |
| Pr(M > NM)        | 0.14                                   | 0.86                                   |

NOTE—Columns are radio-AGN coinciding with an optical AGN determined in [Bilton et al. \(2020\)](#) (AGN<sub>Rad-Opt</sub>) and only radio-AGN (AGN<sub>Rad</sub>). Rows include the total number and the proportion with beta-binomial upper and lower bound uncertainties using a Jeffreys Bayesian prior across both dynamical states. Pr(M > NM) corresponds to the posterior probability that a specific classification is greater in mergers compared to non-mergers, discussed in Section 3.6.

This paper examines the population proportion of radio-AGN morphologies and radio-AGN and optical AGN optical across merging and non-merging clusters. Our findings suggest that mergers have a statistically significant, at a  $3\sigma$  level, increased prevalence of disturbed radio sources and that mergers and non-mergers have a relatively equal prevalence of compact and jetted sources. Notably, a merging cluster environment enables large scale bulk motion in the ICM, increases the potential for more galaxy-galaxy interactions, and heightens the overall disorder in the system. A dynamic environment such as that found in merging systems creates more opportunities for radio jets to interact with their surrounding and become bent ([Morris et al. 2022](#); [O’Dea & Baum 2023](#)) or “disturbed”.

It has already been suggested in the literature that merging cluster systems can affect radio-AGN morphology. There are historically two types of bent-tail radio-AGN: WATs (larger opening angle between the two radio jets) and Narrow Angle Tails (NATs, which have a smaller opening angle between the two radio jets). WATs seem to be fundamentally different from Narrow Angle Tails (NATs) in a variety of ways. The main difference is that WATs are cluster-center objects near the bottom of the cluster potential, and thus WAT host galaxies must be nearly at rest ([Owen & Rudnick 1976](#); [Quintana & Lawrie 1982](#); [Eilek et al. 1984](#)). Therefore, bent WAT morphology cannot be explained by ram pressure due to the motion of the host galaxy. Instead, the WAT bent morphology has been posited to be a result of merging cluster-cluster systems ([Roettiger et al. 1993](#); [Pinkney et al. 1994](#); [Burns 1998](#); [Sakelliou & Merrifield 2000](#); [Burns et al. 2002](#)) where the bulk scale motions

of the ICM are responsible for the ram pressure that bends the tails. And even though there is still debate of the origin of Hybrid Morphology Radio Sources (intrinsic or environmental), an asymmetric environment has been posited as one origin ([Gopal-Krishna & Wiita 2000](#); [Kapińska et al. 2017](#)) which could be created in a cluster-cluster merger ([Gawroński et al. 2006](#)). Therefore, it is not unexpected that a merging system could cause a change in morphology of jetted systems as we see in this work.

We note that we only see head tails in merging systems (see Table 6). Head tails are extreme versions of bent tail systems and are a product of stronger ram pressure either from a denser medium or a higher velocity of the source ( $P_{\text{ram}} = \rho v^2$ ; [Miley et al. 1972](#); [Terni de Gregory et al. 2017](#)). Because only the most disturbed systems (HTs) are found in merging systems, this may indicate that merging systems allow for more opportunities for extreme ram pressure. An interesting follow-up would be to investigate the placement of these head tail systems with respect to the cluster center.

Our findings suggest that mergers have a marginally significant increased prevalence of radio-AGN that are also identified as an optical AGN. If we assume that AGN<sub>Rad</sub> can be roughly equated to an inefficiently accreting engine or low-excitation radio galaxies (LERGs) and the AGN<sub>Rad-Opt</sub> can be roughly equated to an efficiently accreting engine or high-excitation radio galaxies (HERGs) ([Hardcastle et al. 2009](#); [Buttiglione et al. 2010](#); [Best & Heckman 2012](#)) then we see that there are more LERGs than HERGs in merging clusters. Though we do not do a full HERG/LENG classification in this analysis (this was not the goal of this work so potential biases exist such as the fact that this sample was not created to have a S/N target required for detecting the spectral lines needed to classify HERG/LENGs are present), we note that it would be interesting future work. In fact, the environment affecting the incidence of LERGs versus HERGs is not unprecedented. A few early works find that in the local universe LERGs occupy more dense environments than HERGs ([Prestage & Peacock 1988](#); [Allington-Smith et al. 1993](#); [Zirbel 1997](#); [Best 2004](#)), which was confirmed by [Miraghaei & Best \(2017\)](#). On the other hand, [Massaro et al. \(2019, 2020\)](#) do not find a difference in HERG/LENG environments in the local universe and note that the difference in environments of HERGs and LERGs seen in other works could be due to selection bias. However, when [Ineson et al. \(2015\)](#) compare the large-scale environments of HERG and LEGER in the local universe ( $z \sim 1$ ) to that of those at  $z \sim 0.5$ , they do find a difference and note that there

is strong evidence of a difference between the large-scale environments of HERGs and LERGs.

### 5.1. Discussion of Potential Sources of Uncertainty

There are several sources of error which we discuss here. An inherent source of error exists in the limitations of our classifications. Each source presents a unique radio emission profile, and while we aimed to encompass the bulk trends with the classification schemes, some intricacies may have eluded our classification process. Our morphological classification system does not encompass every type of radio galaxy morphology and was not designed to. We acknowledge the presence of jellyfish galaxies in our sample. Notably, we find examples of WC sources exhibiting faint extended emission that do not align exactly with the CE as defined here in this work, but are noteworthy. In fact, two WC sources in Abell 2255 are found in the existing literature to be ram-pressure stripped galaxies (Ignesti et al. 2023). Further we cross-match our sample with the LoTSS jellyfish catalog from Roberts et al. (2021) and we find that four of our radio AGN are identified as jellyfish galaxies. We find that the jellyfish galaxies are equally spread between the WC, SC, CE, and E categories. However we note that the LoTSS jellyfish catalog Roberts et al. (2021) only includes data from LoTSS DR2 data and up to half clusters in this work have LoTSS data that have been taken since DR2. Similarly, we identified sources displaying FR-type morphologies that do not precisely fit FRM or FRI/II categories, potentially due to image artifacts, yet they exhibit distinctive and intriguing morphologies. To maintain the scope of this project, we limit our results to only the original Zooniverse classification results.

An additional source of error that arises inherently in our classification-based project is disagreement. First there are only 71 sources with complete agreement from all classifiers (consensus level 5) and the remaining 90 sources do not have complete agreement. On the other end of the spectrum within our data set, there were 26 sources that did not have a majority agreement (consensus level 2). Involving multiple classifiers was a necessary step to obtain robust classifications, even though it introduces some margin for error. There is a growing movement to move towards having multiple classifications or “tags” per source in the radio classification community in order to better describe the complex nature of the morphology of radio galaxies (Rudnick 2021). For this exploratory work, we chose to have only one classification per object but that leaves room for “error” in that we may not capture the full, complex morphology of the source.

Another source of error is that of the dynamical state classification of the host cluster. It is difficult to obtain a binary classification of the dynamical state of clusters into “merging” and “relaxed.” Galaxy clusters are a direct result of hierarchical merging systems evolving over cosmic time and the clusters we examine are snapshots in time, each characterized by varying degrees of merging activity. There is an ongoing debate surrounding the optimal approach for determining the dynamical state of a galaxy cluster. Our study is based on the Bilton et al. (2020) data set which classifies clusters as merging or non-merging based on a kinematic analysis. However existing literature suggests certain clusters that were classified as a ‘non-merging’ cluster by Bilton et al. (2020) may in fact be undergoing merging processes based on X-ray observations which trace ICM turbulence (Nulsen et al. 2013; Blanton et al. 2011; Bailey et al. 2016; Drabent et al. 2015; Yu et al. 2016; Wen & Han 2013). Another way to classify the dynamical state of a cluster is based on the presence of central radio halos and radio relics which can serve as an effective indicator of ongoing merger events. Notably, at least two clusters (Abell 1367 and Abell 1656) in this sample, classified as non-merging using the Bilton et al. (2020) method, are identified as mergers based on radio halo observations (Kim et al. 1990; Gavazzi 1978; Bonafede et al. 2022; Ge et al. 2019; Zhang et al. 2023).

With these facts in mind, the clusters that Bilton et al. (2020) identified as merging and non-merging via kinematics might not have that classification if one were to use a different type of analysis. Though it is difficult to get uniform, multi-wavelength data for a large sample of clusters, and depending on the science goals, a multi-wavelength approach would be the most robust best way to determine the dynamical state of a cluster.

A last source of error is the choice to use a global RMS for the cutout contours. The choice of a global RMS per cluster, inherently, may lead to the loss of smaller-scale emission for individual sources where the RMS may be different from the global RMS. Given our original dataset from the Bilton et al. (2020) catalog, which comprises over 1000 sources, we were confronted with a trade-off between efficiency and sensitivity. Consequently, emission of lower surface brightness, such as that associated with ram pressure stripping, may not be fully captured. Existing work suggests at least two WC sources from Abell 2255 are ram-pressure stripped galaxies (Ignesti et al. 2023). However, in §3.1 we investigate the effect of choosing global versus a local RMS and find that our choice of a global, cluster RMS does not affect our results.

## 6. SUMMARY

In this work, we explored the effect of galaxy cluster mergers on the radio morphology of radio-AGN. Starting from a sample of 33 galaxy clusters identified as merging (8) or non-merging (25) by [Bilton et al. \(2020\)](#), we assembled a sample of 12 galaxy clusters (8 merging and 4 non-merging) that have LoTSS 144 MHz data. Our method to determine if the merging cluster environment has an effect on radio-AGN morphology was to have 5 experts classify the sources with a radio detection using Zooniverse, according to whether a source is weak compact (WC), strong compact (SC), compact extended (CE), extended (E), FR I or FR II, FR-morphology (FRM), bent tail (BT), or a head tail (HT). We combined the radio morphologies classes into C (WC+SC), CE, E, Jetted (FR I + FR II + FRM), and Disturbed (BT + HT), ( see §4.1), and we obtain the following results:

- mergers do not exhibit a greater proportion of Compact, Compact Extended, and Jetted sources as compared to non-mergers (see §4.1)
- non-mergers contain all the Extended classified sources in this study
- mergers have a statistically significant ( $3\sigma$ ) higher population proportion of Disturbed sources than non-mergers (see §4.1)
- within merging clusters there is a marginally statistically significant ( $2\sigma$ ) higher proportion of AGN that are identified only as radio-AGN compared to radio-AGN that are also identified as an optical AGN (see §4.2)

Overall we find that the merging environment seems to have an effect on the radio morphology of radio sources in that there are more disturbed (bent and head tails) sources in mergers. Our findings suggest the merging environment provides more opportunity for the jets to become disturbed.

We also investigated how the AGN detection fraction changes with wavelength (see §4.2), in particular the fraction of sources that are detected in the radio versus optical. We obtain the following results:

- within merging clusters there is a marginally statistically significant ( $2\sigma$ ) higher proportion of AGN that are identified only as radio-AGN compared to radio-AGN that are also identified as an optical AGN (see §4.2)
- mergers do not exhibit greater proportions of radio-AGNs and radio-AGNs with an optical AGN detection compared to non-mergers.

This study presents significant opportunities for future work. One future direction is to follow a similar analysis as [Bilton et al. \(2020\)](#) and examine the spatial distribution of the classified sources in the phase space diagram. Of particular interest is the potential trends of radio classification at certain spatial cuts within the cluster. A similar future direction would be to investigate the phase space position of the  $\text{AGN}_{\text{Rad}}$  and  $\text{AGN}_{\text{Rad-Opt}}$ . An additional future direction is to extend this work to a larger sample of clusters and have a spectrum of cluster dynamical states. A last future direction would be the further investigation of the "undetermined" or "non-consensus" morphological classifications as there is a significant variation in the morphologies in these morphology classes.

## ACKNOWLEDGEMENTS

We would like to thank the anonymous referee for their useful comments that made this work better. We would also like to thank Drs. Abhijeet Borkar and Paul Martini for helpful discussions. This work was made possible by the support of The National Radio Astronomy Observatory and Green Bank Observatory which are facilities of the U.S. National Science Foundation operated under cooperative agreement by Associated Universities, Inc. M.R. acknowledges support from the Deans' Graduate Fellowship from the University of Notre Dame. Y.A.G. is supported by US National Science Foundation (NSF) grant AST 22-06053. This publication uses data generated via the Zooniverse.org platform, development of which is funded by generous support, including a Global Impact Award from Google, and by a grant from the Alfred P. Sloan Foundation.

*Facilities:* LOFAR (LoTSS)

*Software:* astropy ([Astropy Collaboration et al. 2018](#))

## APPENDIX

### A. ZOONIVERSE RESULTS

We provide a catalog of the 157 classification results following the aggregation of votes from the Zooniverse

**Table 4.** Consensus level 3 example table

| Name                  | Cluster   | D <sub>state</sub> | RA         | DEC       | Radio <sub>class</sub> | RAGN  | OAGN  |
|-----------------------|-----------|--------------------|------------|-----------|------------------------|-------|-------|
| SDSS J031447.7+421321 | ABELL0426 | M                  | 48.698868  | 42.222702 | WC                     | False | False |
| SDSS J114041.6+202034 | ABELL1367 | NM                 | 175.173660 | 20.342951 | WC                     | False | False |
| SDSS J114224.4+200709 | ABELL1367 | NM                 | 175.602066 | 20.119303 | CE                     | False | False |
| SDSS J114358.1+204822 | ABELL1367 | NM                 | 175.992096 | 20.806389 | WC                     | False | False |
| SDSS J114358.9+200437 | ABELL1367 | NM                 | 175.995667 | 20.077028 | CE                     | False | False |
| SDSS J114527.6+204825 | ABELL1367 | NM                 | 176.365280 | 20.807171 | CE                     | False | False |
| SDSS J114548.8+203743 | ABELL1367 | NM                 | 176.453491 | 20.628616 | WC                     | False | False |
| SDSS J114612.1+202329 | ABELL1367 | NM                 | 176.550766 | 20.391647 | SC                     | True  | True  |
| SDSS J115148.4+202727 | ABELL1367 | NM                 | 177.951752 | 20.457710 | WC                     | False | False |
| SDSS J125217.7+270507 | ABELL1656 | NM                 | 193.073837 | 27.085546 | WC                     | False | True  |
| SDSS J125351.5+285845 | ABELL1656 | NM                 | 193.464584 | 28.979395 | WC                     | False | False |
| SDSS J125359.1+262638 | ABELL1656 | NM                 | 193.496307 | 26.444042 | WC                     | False | False |
| SDSS J125455.1+272445 | ABELL1656 | NM                 | 193.729874 | 27.412704 | WC                     | False | False |
| SDSS J125547.8+281521 | ABELL1656 | NM                 | 193.949280 | 28.256104 | WC                     | False | False |
| SDSS J125651.1+265356 | ABELL1656 | NM                 | 194.213211 | 26.898890 | WC                     | False | True  |
| SDSS J125732.8+273637 | ABELL1656 | NM                 | 194.386826 | 27.610346 | WC                     | False | False |
| SDSS J125835.1+273547 | ABELL1656 | NM                 | 194.646606 | 27.596390 | SC                     | False | False |
| SDSS J125855.9+275000 | ABELL1656 | NM                 | 194.733185 | 27.833393 | CE                     | False | False |
| SDSS J125939.1+285343 | ABELL1656 | NM                 | 194.912979 | 28.895521 | WC                     | False | False |
| SDSS J130125.2+291849 | ABELL1656 | NM                 | 195.355286 | 29.313740 | CE                     | True  | True  |

NOTE—The first 20 rows of the full sample of consensus level 3 sources. The full table is provided with this article. Columns are the SDSS name of source [Bilton et al. \(2020\)](#) (Name), the name of the cluster that the source is in (Cluster), the dynamical state of the host cluster, D<sub>state</sub>, which is either non-merging (NM) or merging (M) as defined in [Bilton et al. \(2020\)](#), RA, Dec, the radio classification assigned through the Zooniverse classification done in this work (Radio class, see §3.2), whether or not the source is classified as a radio-AGN (RAGN, see §3.5), and whether or not the source is classified as an optical AGN in [Bilton et al. \(2020\)](#) (OAGN).

**Table 5.** Zooniverse classifications with a consensus level of 3 and above.

|                   | WC | SC | CE | E | FRI+II | FRM | BT | HT | Unc |
|-------------------|----|----|----|---|--------|-----|----|----|-----|
| Tot <sub>NM</sub> | 79 | 19 | 17 | 7 | 1      | 2   | 1  | 0  | 0   |
| Tot <sub>M</sub>  | 19 | 5  | 2  | 0 | 2      | 0   | 1  | 4  | 1   |

NOTE—Column names are shorthand for the classifications detailed in 3.2: weak compact (WC), strong compact (SC), compact extended (CE), extended (E), Fanaroff and Riley I+II (FRI+II), Fanaroff and Riley Morphology (FRM), bent tail (BT), head tail (HT), and uncertain (Unc). Rows detail the total across mergers (M) and non-mergers (NM) for each morphology classification of consensus level of 3 before radio-AGN delineation in section 3.5.

project but prior to combining into bulk group classifications (see §3.4 for details) with this work and display the first 20 lines in Table 4. This does not include differentiation between the source of radio emission from a radio-AGN or star formation.

## B. CONSENSUS LEVEL 3 VS. CONSENSUS LEVEL 4 RESULTS

In Table 6, we present the radio-AGN statistics for consensus level 3 after radio-AGN delineation but before the combined classifications. In Table 7, we observe the consensus level 4 statistics after radio-AGN delineation and before combining classes. In Table 8, we observe the combined classification statistic version of the consensus

**Table 6.** Radio-AGN morphology classifications with a consensus level of 3 and above.

|                   | WC | SC | CE | E | FRI+II | FRM | BT | HT |
|-------------------|----|----|----|---|--------|-----|----|----|
| Tot <sub>NM</sub> | 14 | 8  | 6  | 5 | 1      | 2   | 1  | 0  |
| Tot <sub>M</sub>  | 6  | 3  | 1  | 0 | 2      | 0   | 1  | 4  |

NOTE—Column names are shorthand for the classifications detailed in §3.2 weak compact (WC), strong compact (SC), compact extended (CE), extended (E), Fanaroff and Riley I+II (FRI+II), Fanaroff and Riley Morphology (FRM), bent tail (BT), head tail (HT), and uncertain (Unc). Rows detail the total, average (Avg), and normalized average (Norm) across mergers (M) and non-mergers (NM) for each morphology classification of consensus level of 3 after radio-AGN delineation in section 3.5.

**Table 7.** Radio-AGN morphology classifications with a consensus level of 4 and above.

|                   | WC | SC | CE | E | FRI+II | FRM | BT | HT |
|-------------------|----|----|----|---|--------|-----|----|----|
| Tot <sub>NM</sub> | 10 | 6  | 5  | 2 | 1      | 1   | 0  | 0  |
| Tot <sub>M</sub>  | 6  | 2  | 0  | 0 | 1      | 0   | 0  | 2  |

NOTE—Column names are shorthand for the classifications detailed in §3.2 weak compact (WC), strong compact (SC), compact extended (CE), extended (E), Fanaroff and Riley I+II (FRI+II), Fanaroff and Riley Morphology (FRM), bent tail (BT), head tail (HT). Rows detail the total across mergers (M) and non-mergers (NM) for each morphology classification of consensus level of 4 after radio-AGN delineation.

**Table 8.** Radio-AGN morphology results for combined morphology classes for consensus level 4 and above.

|                   | C                                      | CE                                     | E                                      | Jetted                                 | Disturbed                              |
|-------------------|--|--|--|--|--|
| Tot <sub>NM</sub> | 16                                     | 5                                      | 2                                      | 2                                      | 0                                      |
| Tot <sub>M</sub>  | 8                                      | 0                                      | 0                                      | 1                                      | 2                                      |
| P <sub>NM</sub>   | 0.64 <sup>+0.09</sup> <sub>-0.10</sub> | 0.20 <sup>+0.09</sup> <sub>-0.07</sub> | 0.08 <sup>+0.07</sup> <sub>-0.04</sub> | 0.08 <sup>+0.07</sup> <sub>-0.04</sub> | 0 <sup>+0.03</sup>                     |
| P <sub>M</sub>    | 0.73 <sup>+0.12</sup> <sub>-0.14</sub> | 0 <sup>+0.06</sup>                     | 0 <sup>+0.06</sup>                     | 0.09 <sup>+0.11</sup> <sub>-0.07</sub> | 0.18 <sup>+0.13</sup> <sub>-0.10</sub> |
| Pr(M > NM)        | 0.69                                   | 0.04                                   | 0.19                                   | 0.57                                   | 0.98                                   |

NOTE—Column headers are shorthand for the combined classification groups: Compact (WC+SC), Compact Extended, Extended, Jetted (FRI+FRII+FRM), and Disturbed (HT+BT). Rows describe the total radio-AGN and proportion of the classification within non-mergers and mergers for consensus level 4. Jeffreys Bayesian prior is used to determine the upper and lower bound uncertainty for consensus level 4. Pr(M > NM) corresponds to the posterior probability that a specific classification is greater in mergers compared to non-mergers, discussed in Section 3.6.

level 4 analysis. We determine the results do not change when comparing consensus level 3 and 4. Specifically using the posterior probabilities, we find that mergers do not exhibit statistically significantly greater proportions of either C, CE, E, or Jetted sources compared to non-mergers (in other words, Pr(M>NM) corresponds to a  $\sigma \leq 1$ ). Similarly to consensus level 3, we do find mergers exhibit marginally significant greater proportions of Disturbed sources in consensus level 4, where Pr(M>NM) corresponds to  $\sigma$  of 2.4. We note that we observe no CE or E in the mergers. This differs from

consensus level 3 as we observe no CE sources in consensus level 4, but we attribute this to be resulting from a significant sample size decrease. We also note the population proportion in non-mergers is zero. Sample size plays a significant role in consensus level 4, as it leads to more values consistent with null. While consensus level 4 has a significantly smaller sample size, it still yields similar results as consensus level 3. A change in consensus level changes our result as a higher consensus level drastically reduces our sample size. We decided consensus level 3 was the best for our study to not limit our results due to a small sample size.

## REFERENCES

- Aihara, H., Allende Prieto, C., An, D., et al. 2011, ApJS, 193, 29, doi: [10.1088/0067-0049/193/2/29](https://doi.org/10.1088/0067-0049/193/2/29)
- Alberts, S., Pope, A., Brodwin, M., et al. 2016, ApJ, 825, 72, doi: [10.3847/0004-637X/825/1/72](https://doi.org/10.3847/0004-637X/825/1/72)



- Allington-Smith, J. R., Ellis, R., Zirbel, E. L., & Oemler, Augustus, J. 1993, *ApJ*, 404, 521, doi: [10.1086/172305](https://doi.org/10.1086/172305)
- Astropy Collaboration, Price-Whelan, A. M., Sipőcz, B. M., et al. 2018, *AJ*, 156, 123, doi: [10.3847/1538-3881/aabc4f](https://doi.org/10.3847/1538-3881/aabc4f)
- Bailey, A., Sarazin, C. L., Clarke, T. E., et al. 2016, in *AAS/High Energy Astrophysics Division*, Vol. 15, *AAS/High Energy Astrophysics Division #15*, 111.04
- Baldwin, J. A., Phillips, M. M., & Terlevich, R. 1981, *PASP*, 93, 5, doi: [10.1086/130766](https://doi.org/10.1086/130766)
- Barsanti, S., Owers, M. S., Brough, S., et al. 2018, *ApJ*, 857, 71, doi: [10.3847/1538-4357/aab61a](https://doi.org/10.3847/1538-4357/aab61a)
- Basu, K., Sommer, M., Erler, J., et al. 2016, *ApJL*, 829, L23, doi: [10.3847/2041-8205/829/2/L23](https://doi.org/10.3847/2041-8205/829/2/L23)
- Begelman, M. C., Rees, M. J., & Blandford, R. D. 1979, *Nature*, 279, 770, doi: [10.1038/279770a0](https://doi.org/10.1038/279770a0)
- Best, P. N. 2004, *MNRAS*, 351, 70, doi: [10.1111/j.1365-2966.2004.07752.x](https://doi.org/10.1111/j.1365-2966.2004.07752.x)
- Best, P. N., & Heckman, T. M. 2012, *MNRAS*, 421, 1569, doi: [10.1111/j.1365-2966.2012.20414.x](https://doi.org/10.1111/j.1365-2966.2012.20414.x)
- Best, P. N., Kauffmann, G., Heckman, T. M., & Ivezić, Ž. 2005, *MNRAS*, 362, 9, doi: [10.1111/j.1365-2966.2005.09283.x](https://doi.org/10.1111/j.1365-2966.2005.09283.x)
- Bilton, L. E., Pimblet, K. A., & Gordon, Y. A. 2020, *Monthly Notices of the Royal Astronomical Society*, 499, 3792, doi: [10.1093/mnras/staa3154](https://doi.org/10.1093/mnras/staa3154)
- Blanton, E. L., Randall, S. W., Clarke, T. E., et al. 2011, *ApJ*, 737, 99, doi: [10.1088/0004-637X/737/2/99](https://doi.org/10.1088/0004-637X/737/2/99)
- Bonafede, A., Brunetti, G., Rudnick, L., et al. 2022, *ApJ*, 933, 218, doi: [10.3847/1538-4357/ac721d](https://doi.org/10.3847/1538-4357/ac721d)
- Boylan-Kolchin, M., Springel, V., White, S. D. M., Jenkins, A., & Lemson, G. 2009, *MNRAS*, 398, 1150, doi: [10.1111/j.1365-2966.2009.15191.x](https://doi.org/10.1111/j.1365-2966.2009.15191.x)
- Brinchmann, J., Charlot, S., White, S. D. M., et al. 2004, *MNRAS*, 351, 1151, doi: [10.1111/j.1365-2966.2004.07881.x](https://doi.org/10.1111/j.1365-2966.2004.07881.x)
- Bufanda, E., Hollowood, D., Jeltama, T. E., et al. 2017, *MNRAS*, 465, 2531, doi: [10.1093/mnras/stw2824](https://doi.org/10.1093/mnras/stw2824)
- Buote, D. A. 2002, in *Astrophysics and Space Science Library*, Vol. 272, *Merging Processes in Galaxy Clusters*, ed. L. Feretti, I. M. Gioia, & G. Giovannini, 79–107, doi: [10.1007/0-306-48096-4\\_3](https://doi.org/10.1007/0-306-48096-4_3)
- Burns, J. O. 1998, *Science*, 280, 400, doi: [10.1126/science.280.5362.400](https://doi.org/10.1126/science.280.5362.400)
- Burns, J. O., Loken, C., Roettiger, K., et al. 2002, *NewAR*, 46, 135, doi: [10.1016/S1387-6473\(01\)00168-3](https://doi.org/10.1016/S1387-6473(01)00168-3)
- Buttiglione, S., Capetti, A., Celotti, A., et al. 2010, *A&A*, 509, A6, doi: [10.1051/0004-6361/200913290](https://doi.org/10.1051/0004-6361/200913290)
- Cairns, J., Stroe, A., Breuck, C. D., Mroczkowski, T., & Clements, D. 2019, *The Astrophysical Journal*, 882, 132, doi: [10.3847/1538-4357/ab3392](https://doi.org/10.3847/1538-4357/ab3392)
- Cid Fernandes, R., Stasińska, G., Mateus, A., & Vale Asari, N. 2011, *MNRAS*, 413, 1687, doi: [10.1111/j.1365-2966.2011.18244.x](https://doi.org/10.1111/j.1365-2966.2011.18244.x)
- Cid Fernandes, R., Stasińska, G., Schlickmann, M. S., et al. 2010, *MNRAS*, 403, 1036, doi: [10.1111/j.1365-2966.2009.16185.x](https://doi.org/10.1111/j.1365-2966.2009.16185.x)
- Condon, J. J. 1992, *ARA&A*, 30, 575, doi: [10.1146/annurev.aa.30.090192.003043](https://doi.org/10.1146/annurev.aa.30.090192.003043)
- Croston, J. H., Hardcastle, M. J., Mingo, B., et al. 2019, *A&A*, 622, A10, doi: [10.1051/0004-6361/201834019](https://doi.org/10.1051/0004-6361/201834019)
- De Lucia, G., Poggianti, B. M., Aragón-Salamanca, A., et al. 2004, *ApJL*, 610, L77, doi: [10.1086/423373](https://doi.org/10.1086/423373)
- Diaferio, A. 1999, *MNRAS*, 309, 610, doi: [10.1046/j.1365-8711.1999.02864.x](https://doi.org/10.1046/j.1365-8711.1999.02864.x)
- Diaferio, A., & Geller, M. J. 1997, *ApJ*, 481, 633, doi: [10.1086/304075](https://doi.org/10.1086/304075)
- Drabent, A., Hoeft, M., Pizzo, R. F., et al. 2015, *A&A*, 575, A8, doi: [10.1051/0004-6361/201424828](https://doi.org/10.1051/0004-6361/201424828)
- Dressler, A. 1980, *ApJ*, 236, 351, doi: [10.1086/157753](https://doi.org/10.1086/157753)
- Dressler, A., & Shectman, S. A. 1988, *AJ*, 95, 985, doi: [10.1086/114694](https://doi.org/10.1086/114694)
- Ebeling, H., Stephenson, L. N., & Edge, A. C. 2014, *ApJL*, 781, L40, doi: [10.1088/2041-8205/781/2/L40](https://doi.org/10.1088/2041-8205/781/2/L40)
- Ehlert, S., von der Linden, A., Allen, S. W., et al. 2014, *MNRAS*, 437, 1942, doi: [10.1093/mnras/stt2025](https://doi.org/10.1093/mnras/stt2025)
- Eilek, J. A., Burns, J. O., O’Dea, C. P., & Owen, F. N. 1984, *ApJ*, 278, 37, doi: [10.1086/161765](https://doi.org/10.1086/161765)
- Fanaroff, B. L., & Riley, J. M. 1974, *MNRAS*, 167, 31P, doi: [10.1093/mnras/167.1.31P](https://doi.org/10.1093/mnras/167.1.31P)
- Fassbender, R., Šuhada, R., & Nastasi, A. 2012, *Advances in Astronomy*, 2012, 138380, doi: [10.1155/2012/138380](https://doi.org/10.1155/2012/138380)
- Fassbender, R., Nastasi, A., Santos, J. S., et al. 2014, *A&A*, 568, A5, doi: [10.1051/0004-6361/201423941](https://doi.org/10.1051/0004-6361/201423941)
- Fujita, Y. 1998, *ApJ*, 509, 587, doi: [10.1086/306518](https://doi.org/10.1086/306518)
- Fumagalli, M., Fossati, M., Hau, G. K. T., et al. 2014, *MNRAS*, 445, 4335, doi: [10.1093/mnras/stu2092](https://doi.org/10.1093/mnras/stu2092)
- Galametz, A., Stern, D., Eisenhardt, P. R. M., et al. 2009, *ApJ*, 694, 1309, doi: [10.1088/0004-637X/694/2/1309](https://doi.org/10.1088/0004-637X/694/2/1309)
- Garon, A. F., Rudnick, L., Wong, O. I., et al. 2019, *AJ*, 157, 126, doi: [10.3847/1538-3881/aaff62](https://doi.org/10.3847/1538-3881/aaff62)
- Gavazzi, G. 1978, *A&A*, 69, 355
- Gawroński, M. P., Marecki, A., Kunert-Bajraszewska, M., & Kus, A. J. 2006, *A&A*, 447, 63, doi: [10.1051/0004-6361:20053996](https://doi.org/10.1051/0004-6361:20053996)
- Ge, C., Sun, M., Liu, R.-Y., et al. 2019, *MNRAS*, 486, L36, doi: [10.1093/mnrasl/slz049](https://doi.org/10.1093/mnrasl/slz049)
- Gendre, M. A., Best, P. N., Wall, J. V., & Ker, L. M. 2013, *MNRAS*, 430, 3086, doi: [10.1093/mnras/stt116](https://doi.org/10.1093/mnras/stt116)
- Gifford, D., Miller, C., & Kern, N. 2013, *ApJ*, 773, 116, doi: [10.1088/0004-637x/773/2/116](https://doi.org/10.1088/0004-637x/773/2/116)

- Gifford, D., & Miller, C. J. 2013, *ApJL*, 768, L32, doi: [10.1088/2041-8205/768/2/L32](https://doi.org/10.1088/2041-8205/768/2/L32)
- Gopal-Krishna, & Wiita, P. J. 2000, *A&A*, 363, 507. <https://arxiv.org/abs/astro-ph/0009441>
- Gordon, Y. A., Pimblet, K. A., Owers, M. S., et al. 2018, *MNRAS*, 475, 4223, doi: [10.1093/mnras/sty115](https://doi.org/10.1093/mnras/sty115)
- Gunn, J. E., & Gott, J. Richard, I. 1972, *ApJ*, 176, 1, doi: [10.1086/151605](https://doi.org/10.1086/151605)
- Gürkan, G., Hardcastle, M. J., Smith, D. J. B., et al. 2018, *MNRAS*, 475, 3010, doi: [10.1093/mnras/sty016](https://doi.org/10.1093/mnras/sty016)
- Hardcastle, M. J., Evans, D. A., & Croston, J. H. 2009, *MNRAS*, 396, 1929, doi: [10.1111/j.1365-2966.2009.14887.x](https://doi.org/10.1111/j.1365-2966.2009.14887.x)
- Hardcastle, M. J., Sakelliou, I., & Worrall, D. M. 2005, *MNRAS*, 359, 1007, doi: [10.1111/j.1365-2966.2005.08966.x](https://doi.org/10.1111/j.1365-2966.2005.08966.x)
- Hwang, H. S., & Lee, M. G. 2009, *MNRAS*, 397, 2111, doi: [10.1111/j.1365-2966.2009.15100.x](https://doi.org/10.1111/j.1365-2966.2009.15100.x)
- Ignesti, A., Vulcani, B., Botteon, A., et al. 2023, *A&A*, 675, A118, doi: [10.1051/0004-6361/202346517](https://doi.org/10.1051/0004-6361/202346517)
- Ineson, J., Croston, J. H., Hardcastle, M. J., et al. 2015, *MNRAS*, 453, 2682, doi: [10.1093/mnras/stv1807](https://doi.org/10.1093/mnras/stv1807)
- Jaffé, Y. L., Poggianti, B. M., Moretti, A., et al. 2018, *MNRAS*, 476, 4753, doi: [10.1093/mnras/sty500](https://doi.org/10.1093/mnras/sty500)
- Joye, W. A., & Mandel, E. 2003, in *Astronomical Society of the Pacific Conference Series*, Vol. 295, *Astronomical Data Analysis Software and Systems XII*, ed. H. E. Payne, R. I. Jedrzejewski, & R. N. Hook, 489
- Kapińska, A. D., Terentev, I., Wong, O. I., et al. 2017, *AJ*, 154, 253, doi: [10.3847/1538-3881/aa90b7](https://doi.org/10.3847/1538-3881/aa90b7)
- Kauffmann, G., White, S. D. M., Heckman, T. M., et al. 2004, *MNRAS*, 353, 713, doi: [10.1111/j.1365-2966.2004.08117.x](https://doi.org/10.1111/j.1365-2966.2004.08117.x)
- Kauffmann, G., Heckman, T. M., White, S. D. M., et al. 2003, *MNRAS*, 341, 33, doi: [10.1046/j.1365-8711.2003.06291.x](https://doi.org/10.1046/j.1365-8711.2003.06291.x)
- Kim, K. T., Kronberg, P. P., Dewdney, P. E., & Landecker, T. L. 1990, *ApJ*, 355, 29, doi: [10.1086/168737](https://doi.org/10.1086/168737)
- Klypin, A. A., Trujillo-Gomez, S., & Primack, J. 2011, *ApJ*, 740, 102, doi: [10.1088/0004-637X/740/2/102](https://doi.org/10.1088/0004-637X/740/2/102)
- Kodama, T., Smail, I., Nakata, F., Okamura, S., & Bower, R. G. 2001, *ApJL*, 562, L9, doi: [10.1086/338100](https://doi.org/10.1086/338100)
- Larson, R. B., Tinsley, B. M., & Caldwell, C. N. 1980, *ApJ*, 237, 692, doi: [10.1086/157917](https://doi.org/10.1086/157917)
- Lintott, C. J., Schawinski, K., Slosar, A., et al. 2008, *MNRAS*, 389, 1179, doi: [10.1111/j.1365-2966.2008.13689.x](https://doi.org/10.1111/j.1365-2966.2008.13689.x)
- Macconi, D., Torresi, E., Grandi, P., Boccardi, B., & Vignali, C. 2020, *MNRAS*, 493, 4355, doi: [10.1093/mnras/staa560](https://doi.org/10.1093/mnras/staa560)
- Mansheim, A. S., Lemaux, B. C., Tomczak, A. R., et al. 2017, *Monthly Notices of the Royal Astronomical Society: Letters*, 469, L20, doi: [10.1093/mnrasl/slx041](https://doi.org/10.1093/mnrasl/slx041)
- Margoniner, V. E., de Carvalho, R. R., Gal, R. R., & Djorgovski, S. G. 2001, *ApJL*, 548, L143, doi: [10.1086/319099](https://doi.org/10.1086/319099)
- Markevitch, M. 2006, in *ESA Special Publication*, Vol. 604, *The X-ray Universe 2005*, ed. A. Wilson, 723, doi: [10.48550/arXiv.astro-ph/0511345](https://doi.org/10.48550/arXiv.astro-ph/0511345)
- Marshall, M. A., Shabala, S. S., Krause, M. G. H., et al. 2018, *MNRAS*, 474, 3615, doi: [10.1093/mnras/stx2996](https://doi.org/10.1093/mnras/stx2996)
- Martini, P., Miller, E. D., Brodwin, M., et al. 2013, *ApJ*, 768, 1, doi: [10.1088/0004-637X/768/1/1](https://doi.org/10.1088/0004-637X/768/1/1)
- Massaro, F., Álvarez-Crespo, N., Capetti, A., et al. 2019, *ApJS*, 240, 20, doi: [10.3847/1538-4365/aaf1c7](https://doi.org/10.3847/1538-4365/aaf1c7)
- Massaro, F., Capetti, A., Paggi, A., et al. 2020, *ApJS*, 247, 71, doi: [10.3847/1538-4365/ab799e](https://doi.org/10.3847/1538-4365/ab799e)
- Miley, G. K., Perola, G. C., van der Kruit, P. C., & van der Laan, H. 1972, *Nature*, 237, 269, doi: [10.1038/237269a0](https://doi.org/10.1038/237269a0)
- Miller, N., & Owen, F. 2003, *The Astronomical Journal*, 125, 2427, doi: [10.1086/374767](https://doi.org/10.1086/374767)
- Miraghaei, H., & Best, P. N. 2017, *MNRAS*, 466, 4346, doi: [10.1093/mnras/stx007](https://doi.org/10.1093/mnras/stx007)
- Mo, W., Gonzalez, A., Stern, D., et al. 2018, *ApJ*, 869, 131, doi: [10.3847/1538-4357/aaef83](https://doi.org/10.3847/1538-4357/aaef83)
- Mo, W., Gonzalez, A., Brodwin, M., et al. 2020, *ApJ*, 901, 131, doi: [10.3847/1538-4357/abb08d](https://doi.org/10.3847/1538-4357/abb08d)
- Mohan, N., & Rafferty, D. 2015, *PyBDSF: Python Blob Detection and Source Finder*, *Astrophysics Source Code Library*, record ascl:1502.007. <http://ascl.net/1502.007>
- Moore, B., Katz, N., Lake, G., Dressler, A., & Oemler, A. 1996, *Nature*, 379, 613, doi: [10.1038/379613a0](https://doi.org/10.1038/379613a0)
- Moore, B., Lake, G., Quinn, T., & Stadel, J. 1999, *MNRAS*, 304, 465, doi: [10.1046/j.1365-8711.1999.02345.x](https://doi.org/10.1046/j.1365-8711.1999.02345.x)
- Moravec, E., Gonzalez, A. H., Stern, D., et al. 2020, *ApJ*, 888, 74, doi: [10.3847/1538-4357/ab5faf](https://doi.org/10.3847/1538-4357/ab5faf)
- Moravec, E., Gonzalez, A. H., Dicker, S., et al. 2020, *The Astrophysical Journal*, 898, 145, doi: [10.3847/1538-4357/aba0b2](https://doi.org/10.3847/1538-4357/aba0b2)
- Morris, M. E., Wilcots, E., Hooper, E., & Heinz, S. 2022, *AJ*, 163, 280, doi: [10.3847/1538-3881/ac66db](https://doi.org/10.3847/1538-3881/ac66db)
- Morsony, B. J., Miller, J. J., Heinz, S., et al. 2013, *MNRAS*, 431, 781, doi: [10.1093/mnras/stt210](https://doi.org/10.1093/mnras/stt210)
- Mroczkowski, T., Nagai, D., Basu, K., et al. 2019, *SSRv*, 215, 17, doi: [10.1007/s11214-019-0581-2](https://doi.org/10.1007/s11214-019-0581-2)
- Natarajan, P., Kneib, J.-P., Smail, I., & Ellis, R. S. 1998, *ApJ*, 499, 600, doi: [10.1086/305660](https://doi.org/10.1086/305660)
- Noordeh, E., Canning, R. E. A., King, A., et al. 2020, *Monthly Notices of the Royal Astronomical Society*, 498, 4095, doi: [10.1093/mnras/staa2682](https://doi.org/10.1093/mnras/staa2682)

- Nulsen, P. E. J., Li, Z., Forman, W. R., et al. 2013, *ApJ*, 775, 117, doi: [10.1088/0004-637X/775/2/117](https://doi.org/10.1088/0004-637X/775/2/117)
- O’Dea, C. P., & Baum, S. A. 2023, *Galaxies*, 11, 67, doi: [10.3390/galaxies11030067](https://doi.org/10.3390/galaxies11030067)
- O’Dea, C. P., & Owen, F. N. 1985, *AJ*, 90, 954, doi: [10.1086/113802](https://doi.org/10.1086/113802)
- O’Donoghue, A. A., Eilek, J. A., & Owen, F. N. 1993, *ApJ*, 408, 428, doi: [10.1086/172600](https://doi.org/10.1086/172600)
- Owen, F. N., Ledlow, M. J., Keel, W. C., & Morrison, G. E. 1999, *The Astronomical Journal*, 118, 633, doi: [10.1086/300974](https://doi.org/10.1086/300974)
- Owen, F. N., & Rudnick, L. 1976, *ApJL*, 205, L1, doi: [10.1086/182077](https://doi.org/10.1086/182077)
- Owers, M. S., Nulsen, P. E. J., Couch, W. J., & Markevitch, M. 2009, *ApJ*, 704, 1349, doi: [10.1088/0004-637X/704/2/1349](https://doi.org/10.1088/0004-637X/704/2/1349)
- Padovani, P., Alexander, D. M., Assef, R. J., et al. 2017, *A&A Rv*, 25, 2, doi: [10.1007/s00159-017-0102-9](https://doi.org/10.1007/s00159-017-0102-9)
- Pillepich, A., Springel, V., Nelson, D., et al. 2018, *MNRAS*, 473, 4077, doi: [10.1093/mnras/stx2656](https://doi.org/10.1093/mnras/stx2656)
- Pimblet, K. A., Shabala, S. S., Haines, C. P., Fraser-McKelvie, A., & Floyd, D. J. E. 2013, *MNRAS*, 429, 1827, doi: [10.1093/mnras/sts470](https://doi.org/10.1093/mnras/sts470)
- Pinkney, J., Burns, J. O., & Hill, J. M. 1994, *AJ*, 108, 2031, doi: [10.1086/117216](https://doi.org/10.1086/117216)
- Planck Collaboration, Aghanim, N., Akrami, Y., et al. 2020, *A&A*, 641, A6, doi: [10.1051/0004-6361/201833910](https://doi.org/10.1051/0004-6361/201833910)
- Poggianti, B. M., von der Linden, A., De Lucia, G., et al. 2006, *ApJ*, 642, 188, doi: [10.1086/500666](https://doi.org/10.1086/500666)
- Poggianti, B. M., Jaffé, Y. L., Moretti, A., et al. 2017, *Nature*, 548, 304, doi: [10.1038/nature23462](https://doi.org/10.1038/nature23462)
- Prestage, R. M., & Peacock, J. A. 1988, *MNRAS*, 230, 131, doi: [10.1093/mnras/230.1.131](https://doi.org/10.1093/mnras/230.1.131)
- Quintana, H., & Lawrie, D. G. 1982, *AJ*, 87, 1, doi: [10.1086/113080](https://doi.org/10.1086/113080)
- Roberts, I. D., van Weeren, R. J., McGee, S. L., et al. 2021, *A&A*, 650, A111, doi: [10.1051/0004-6361/202140784](https://doi.org/10.1051/0004-6361/202140784)
- Roediger, E., Kraft, R. P., Forman, W. R., Nulsen, P. E. J., & Churazov, E. 2013, *ApJ*, 764, 60, doi: [10.1088/0004-637X/764/1/60](https://doi.org/10.1088/0004-637X/764/1/60)
- Roettiger, K., Burns, J., & Loken, C. 1993, *ApJL*, 407, L53, doi: [10.1086/186804](https://doi.org/10.1086/186804)
- Ruderman, J. T., & Ebeling, H. 2005, *ApJL*, 623, L81, doi: [10.1086/430131](https://doi.org/10.1086/430131)
- Rudnick, G., von der Linden, A., Pelló, R., et al. 2009, *ApJ*, 700, 1559, doi: [10.1088/0004-637X/700/2/1559](https://doi.org/10.1088/0004-637X/700/2/1559)
- Rudnick, L. 2021, *Galaxies*, 9, 85, doi: [10.3390/galaxies9040085](https://doi.org/10.3390/galaxies9040085)
- Sadat, R., Blanchard, A., Kneib, J.-P., et al. 2004, *A&A*, 424, 1097, doi: [10.1051/0004-6361:20034029](https://doi.org/10.1051/0004-6361:20034029)
- Saintonge, A., Tran, K.-V. H., & Holden, B. P. 2008, *ApJL*, 685, L113, doi: [10.1086/592730](https://doi.org/10.1086/592730)
- Sakelliou, I., & Merrifield, M. R. 2000, *MNRAS*, 311, 649, doi: [10.1046/j.1365-8711.2000.03079.x](https://doi.org/10.1046/j.1365-8711.2000.03079.x)
- Salim, S., Rich, R. M., Charlot, S., et al. 2007, *ApJS*, 173, 267, doi: [10.1086/519218](https://doi.org/10.1086/519218)
- Sarazin, C. L. 2002, in *Astrophysics and Space Science Library*, Vol. 272, *Merging Processes in Galaxy Clusters*, ed. L. Feretti, I. M. Gioia, & G. Giovannini, 1–38, doi: [10.1007/0-306-48096-4\\_1](https://doi.org/10.1007/0-306-48096-4_1)
- Sazonova, E., Alatalo, K., Lotz, J., et al. 2020, *ApJ*, 899, 85, doi: [10.3847/1538-4357/aba42f](https://doi.org/10.3847/1538-4357/aba42f)
- Shen, L., Liu, G., Zhang, M.-F., et al. 2020, *ApJ*, 902, 101, doi: [10.3847/1538-4357/abb5a0](https://doi.org/10.3847/1538-4357/abb5a0)
- Shimwell, T. W., Röttgering, H. J. A., Best, P. N., et al. 2017, *A&A*, 598, A104, doi: [10.1051/0004-6361/201629313](https://doi.org/10.1051/0004-6361/201629313)
- Shimwell, T. W., Hardcastle, M. J., Tasse, C., et al. 2022, *A&A*, 659, A1, doi: [10.1051/0004-6361/202142484](https://doi.org/10.1051/0004-6361/202142484)
- Smith, R. J., Hudson, M. J., Nelan, J. E., et al. 2004, *AJ*, 128, 1558, doi: [10.1086/423915](https://doi.org/10.1086/423915)
- Sobral, D., Stroe, A., Dawson, W. A., et al. 2015, *MNRAS*, 450, 630, doi: [10.1093/mnras/stv521](https://doi.org/10.1093/mnras/stv521)
- Springel, V., White, S. D. M., Jenkins, A., et al. 2005, *Nature*, 435, 629, doi: [10.1038/nature03597](https://doi.org/10.1038/nature03597)
- Strauss, M. A., Weinberg, D. H., Lupton, R. H., et al. 2002, *AJ*, 124, 1810, doi: [10.1086/342343](https://doi.org/10.1086/342343)
- Stroe, A., Sobral, D., Dawson, W., et al. 2015, *Monthly Notices of the Royal Astronomical Society*, 450, 646, doi: [10.1093/mnras/stu2519](https://doi.org/10.1093/mnras/stu2519)
- Terni de Gregory, B., Feretti, L., Giovannini, G., et al. 2017, *A&A*, 608, A58, doi: [10.1051/0004-6361/201730878](https://doi.org/10.1051/0004-6361/201730878)
- Voit, G. M. 2005, *Reviews of Modern Physics*, 77, 207, doi: [10.1103/RevModPhys.77.207](https://doi.org/10.1103/RevModPhys.77.207)
- Walker, S. A., Fabian, A. C., Sanders, J. S., George, M. R., & Tawara, Y. 2012, *MNRAS*, 422, 3503, doi: [10.1111/j.1365-2966.2012.20860.x](https://doi.org/10.1111/j.1365-2966.2012.20860.x)
- Wen, Z. L., & Han, J. L. 2013, *MNRAS*, 436, 275, doi: [10.1093/mnras/stt1581](https://doi.org/10.1093/mnras/stt1581)
- Yoon, J. H., Schawinski, K., Sheen, Y.-K., Ree, C. H., & Yi, S. K. 2008, *ApJS*, 176, 414, doi: [10.1086/528958](https://doi.org/10.1086/528958)
- York, D. G., Adelman, J., Anderson, John E., J., et al. 2000, *AJ*, 120, 1579, doi: [10.1086/301513](https://doi.org/10.1086/301513)
- Yu, H., Diaferio, A., Agulli, I., Aguerri, J. A. L., & Tozzi, P. 2016, *ApJ*, 831, 156, doi: [10.3847/0004-637X/831/2/156](https://doi.org/10.3847/0004-637X/831/2/156)
- Zhang, C., Zhuravleva, I., Churazov, E., et al. 2023, in *AAS/High Energy Astrophysics Division*, Vol. 20, *AAS/High Energy Astrophysics Division*, 101.05
- Zirbel, E. L. 1997, *ApJ*, 476, 489, doi: [10.1086/303626](https://doi.org/10.1086/303626)